UK Vertical Lift Network

3rd Annual Technical Workshop

Shrigley Hall Hotel, Cheshire

22nd – 23rd May 2017

Supported by:

EPSRC
Pioneering research and skills

Programme & Book of Abstracts

UK Vertical Lift Network: 3rd Technical Workshop

Welcome to the UK VLN Technical Workshop, an annual event showcasing the UK's cutting edge research in rotary wing research. Now in its third year, this event provides a platform for technical discussions on all things *rotorcraft,* from whirl flutter to active twist. For the second year running, we meet at picturesque Shrigley Hall Country House, nestled in the Cheshire hills overlooking Greater Manchester to the north.

We would like to thank all our presenters, who have provided the abstracts contain herewith in. The programme for these two days consists of 19 presentations on a range of subjects. This is an increase on last year, which shows that we are moving on a positive gradient, growing the rotorcraft research community – one of the core aims of the Vertical Lift Network.

Traditionally, the programme of presentations has been categorised by the traditional research areas: aerodynamics, dynamics, flight mechanics and so on. However, this year we have decided to group the sessions according to more specific subject areas, to reflect the multi-disciplinary nature of rotorcraft research and draw attention to some of the key challenges in the field. We have a total of seven sessions running consecutively over the next two days:

- Whirl Flutter
- Propellers
- Flow Control
- Operations & Handling
- Wake Interaction
- Active Rotors
- Sensing & Measurement

We once again welcome our colleagues from industry to the technical workshop. Leonardo Helicopters and DSTL are actively engaged in rotorcraft research and have on-going collaborations with academic partners within the VLN. This healthy interaction demonstrates that our field is truly impactful and naturally collaborative. We thank our industrial VLN members for their time and contributions.

The purpose of this workshop is not limited to the presentation of on-going research; it is also a forum to exchange views and promote new ideas in a relaxing environment. We anticipate that this will stimulate discussion and further catalyse the growth of rotorcraft research in the UK.

We do hope you enjoy the technical workshop.

Nicholas Bojdo and Antonio Filippone
The University of Manchester
9th May 2017

The 3rd Annual UK Vertical Lift Network Technical Workshop

Shrigley Hall Hotel, Cheshire

22-23 May 2017

UK Vertical Lift Network

BAT - University of Bath	LEO - Leonardo Helicopters
BRI - University of Bristol	LIV - University of Liverpool
CRA - Cranfield University	MAN - University of Manchester
GLA - University of Glasgow	DSTL - Defence Science & Technology Laboratories

Final Programme

Monday 22nd May

09.30 - 10.00	Coffee			
10.00 - 10.20	**Keynote**	Antonio Filippone	MAN	*Introduction : Update on the UK Vertical Lift Network*
10.20 - 10.45	**Whirl Flutter**	Higgins, Ross	GLA	*Whirl Flutter Simulation Using CFD*
11.10 - 11.35		Mair, Chris	BRI	*Review of whirl flutter models and stability analysis*
11.35 - 12.00	**Propellers**	Chirico, Giulia	GLA	*Aeroacoustic Analysis of Modern Propeller Designs*
12.00 - 12.25		Smith, Dale	MAN	*Counter Rotating Open Rotors for General Aviation*
12.25 - 13.30	Lunch			
13.30 - 13.55	**Flow Control**	Liu, Xiao	BRI	*Noise Control for a Trailing-edge Serrated Aifroil in Tandem Configuration*
14.20 - 14.45		Green, Richard	GLA	*Delay of dynamic stall using pulsed air jet vortex generators*
14.45 - 15.10		deHaeze, Florent	LEO	*CFD Methods Development for the Simulation of Tilt Rotor Aircraft in the HiPerTilt Project*
15.10 - 15.30	Coffee			
15.00 - 15.25	**Operations & Handling**	Memon, Wajih	LIV	*Heliflight-R Rotorcraft Simulator Fidelity Research*
15.25 - 15.50		Taylor, Neil	DSTL	*DSTL Rotorcraft Research Priorities*
15.50 - 18.30	**Country Walk**	All		
18.30 - 20.00	Dinner			

Tuesday 23rd May

07.00 - 08.30	Breakfast			
08.30 - 09.00	Coffee			
09.00 - 09.25	**Wake Interaction**	Jimenez-Garcia, Antonio	GLA	*A High-Order Method for Rotorcraft Flow*
09.25 - 09.50		Tan, Jianfeng	GLA	*Analysis of Unsteady Aerodynamic Load of Tail Rotor under Main Rotor Aerodynamic Interaction with Vortex Method*
09.50 - 10.15		Appleton, Wesley	MAN	*Aermechanics of Tilrotor Aircraft*
10.15 - 10.40		Watson, Neal	LIV	*Numerical and Experimental Comparison of a Carrier Air-wake for use in Fixed-Wing and Rotary-Wing Flight Simulation*
10.40 - 11.00	Coffee			
11.00 - 11.25	**Active Rotors**	Magowan, Thomas	LEO	*Vibration Control Development and System Integration for an Active Trailing Edge System to Reduce Helicopter Noise and Vibration*
11.25 - 11.50		Woodgate, Mark	GLA	*Active Blade Twist and Advanced Rotor Tip Design*
11.50 - 12.15		Rivero, Andres	BRI	*Analytical Modeling of a Composite Fish Bone Active Camber Morphing Aerofoil*
12.15 - 13.30	Lunch			
13.30 - 13.55	**Sensing & Measurement**	Barbini, Leonardo	BATH	*Detection of a defective bearing on a civil aircraft engine*
13.55 - 14.20		Furtado, Samuel	MAN	*Structural Design, Manufacturing and Instrumentation of rotor blades*
14.20 - 14.45		Lone, Mussadir	CRA	*An update of the BLADESENSE project*
14.45 - 15.10	Coffee			
15.10 - 16.00	**Closing Session**	All		

Book of Abstracts

Whirl Flutter Simulation Using CFD

Ross J. Higgins * and George N. Barakos †

Whirl flutter are potentially dangerous phenomena for turboprop aircraft and tiltrotors . For this reason, the present work is looking at methods to predict the onset of flutter and mitigate its effects.

The first observations of whirl flutter were made in the thirties within turboprop aircraft but serious studies followed some ten years after. The phenomenon was also studied for tiltrotor aircraft, and recent works [1] tend to build on the tests performed by NASA at the Langley facilities. [2, 3, 4, 5]

Most studies, so far, use decoupled aerodynamics, however an investigation into the coupling of complex structural models and CFD generated aerodynamics has been conducted in 2016 [6].The present work deals with coupling between CFD and structural models for whirl flutter. A multi-body dynamics model (Figure 1) is used, coupled with CFD-generated aerodynamics. This multi-body dynamics model incorporates two modes of pitch (θ) and yaw (ψ). Incorportated within this model is the propeller rotational velocity (Ω), the rotational engine attachment stiffnesses within pitch and yaw (k_θ and k_ψ, respectively), structural damping in pitch and yaw (γ_θ and γ_ψ, respectively) and aerodynamic lateral forces and moments (P_Y and $M_{Y,P}$, respectively) and pitching forces and moments (P_Z and $M_{Z,P}$, respectively) of the propeller. The distance from engine attachment to propeller is denoted by a. This tool is validated using a step-by-step approach using data from the open literature [7].

Based upon the multi-body dynamics model shown in Figure 1, the whirl flutter equation of motion is derived via Lagrange's equation and is shown in Equation 1, where the mass matrix ($\mathbf{M}$), structural damping matrix ($\mathbf{D}$), structural stiffness matrix ($\mathbf{K}$), gyroscopic matrix ($\mathbf{G}$), aerodynamic damping ($\mathbf{D^A}$), and stiffness matricies ($\mathbf{K_A}$) are defined. This equation of motion is a quadratic function in terms of the angular velocity (ω), with an imaginary unit, j, due to the damping component within the system. The dynamic head (q_∞), freestream velocity (V_∞), and propeller disc area (F_p) and diameter (D_p) are also taken into account.

$$\left(-\omega^2\left[\mathbf{M}\right]+j\omega\left(\left[\mathbf{D}\right]+\left[\mathbf{G}\right]+q_\infty F_p\frac{D_p^2}{V_\infty}\left[\mathbf{D^A}\right]\right)+\left(\left[\mathbf{K}\right]+q_\infty F_p D_p\left[\mathbf{K^A}\right]\right)\right)\left|\frac{\Theta}{\Psi}\right|=\{0\} \tag{1}$$

An eigenvalue analysis was conducted using this model and Figure 2 shows the results with de-coupled aerodynamics for a four-bladed propeller with variable chord.

References

[1] Kreshock, A. and Yeo, H., "Tiltrotor Whirl-Flutter Stability Predictions Using Comprehensive Analysis," *28th AIAA/ASCE/AHS/ASC Structures, Structural Dynamics, and Materials Conference*, AIAA SciTech Forum, January 2017.

*PhD Student - r.higgins.1@research.gla.ac.uk - CFD Laboratory, School of Engineering, University of Glasgow, G12 8QQ, UK

†Professor - George.Barakos@glasgow.ac.uk - CFD Laboratory, School of Engineering, University of Glasgow, G12 8QQ, UK

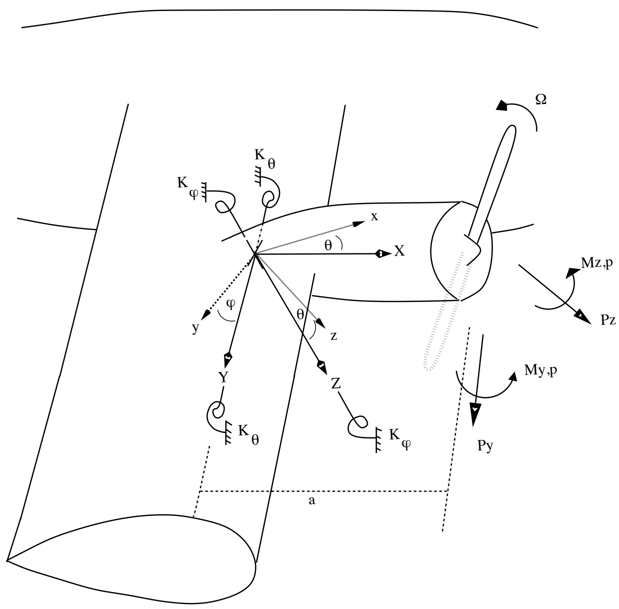

Figure 1: Schematic of the whirl flutter setup built in the multi-body dynamics model

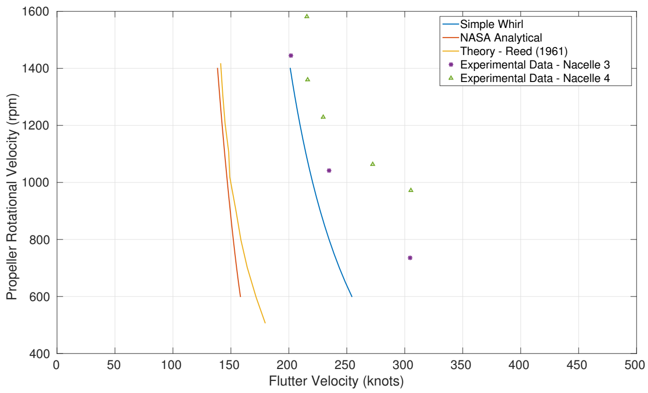

Figure 2: Whirl flutter boundary

[2] Reed, W. and Bland, S., "An Analytical Treatment of Aircraft Propeller Precession Instability," Tech. Rep. D-659, National Aeronautics and Space Administration, January 1961.

[3] Abbott, F., Kelly, H., and Hampton, K., "Investigation of Propeller-Power-Plant Autoprecession Boundaries for a Dynamic-Aeroelastic Model of a Four-Engine Turboprop Transport Airplane," Tech. Rep. D-1806, National Aeronautics and Space Administration, August 1963.

[4] Bland, S. and Bennett, R., "Wind-Tunnel Measurement of Propeller Whirl-Flutter Speeds and Static Stability Derivatives and Comparison with Theory," Tech. Rep. D-1807, National Aeronautics and Space Administration, August 1963.

[5] Bennett, R. and Bland, S., "Experimental and Analytical Investigation of Propeller Whirl Flutter of a Power Plant on a Flexible Wing," Tech. Rep. D-2399, National Aeronautics and Space Administration, August 1964.

[6] Leble, V. and Barakos, G., "Demonstration of a coupled floating offshore wind turbine analysis with high-fidelity methods," *Journal of Fluids and Structures*, Vol. 62, 2016.

[7] Cecrdle, J., *Whirl Flutter of Turboprop Aircraft Structures*, Woodhead Publishing, 1st ed., 2015.

Review of whirl flutter models and stability analysis methods for nonlinear tiltrotor application

Chris Mair[1], Dr Djamel Rezgui[2] and Dr Branislav Titurus[3]

Department of Aerospace Engineering,

University of Bristol, Queens Building, Bristol, UK

Summary

Whirl flutter is an aeroelastic instability that affects several vehicles, including tiltrotors. Tiltrotors with the capacity of regional jets could present a solution to the problem of congestion at airports, though it is not known how nonlinear effects scale with size. Furthermore, whirl flutter limits the maximum speed of current tiltrotor models[1] and therefore their productivity, heightening the importance of adequate modelling and prediction tools. This paper presents a review of existing models and stability analysis methods used since whirl flutter became an aircraft design consideration. The investigation covers older approaches derived by W. H. Reed to newer CAMRAD models, and uses MATLAB code to illustrate models used where possible.

The paper is intended to stimulate discussion regarding the relative merits and drawbacks of the various approaches used in both models and methods, and demonstrate the impact of nonlinearity on a tiltrotor wing-nacelle system's behaviour and stability.

Introduction

Tiltrotors such as the ERICA tiltrotor shown in Figure 1 are a technology area of growing importance due to their potential solution of the airport congestion problem worldwide. If tiltrotors with the passenger capacity of a regional jet can be developed, then regional jet traffic can be offloaded from the runways and transferred to helipads that most airports are already equipped with. In addition to the fact that this desired size of tiltrotor is substantially larger than any existing models, a further challenge is ensuring accurate aeroelastic modelling to protect against an instability known as whirl flutter.

Whirl flutter in its most common context involves a rotor or propeller mounted in a wing nacelle, the hub of which whirls in a circle around its nominal position. Aerodynamic forces acting on the blades and gyroscopic effects acting on the rotor as a whole can couple with wing modes to produce an unstable vibration which can damage or even destroy the aircraft structure. With their large and flexible blades, tiltrotors are particularly susceptible, and whirl flutter generally limits their maximum cruise speed.

Traditional eigenvalue analysis can be used to assess the stability of linear systems, however for nonlinear systems bifurcation and continuation methods can give a more complete insight, particularly when stability boundaries are required.

[1] PhD Student, University of Bristol, chris.mair@my.bristol.ac.uk
[2] Lecturer in Aerospace Engineering, University of Bristol, djamel.rezgui@bristol.ac.uk
[3] Lecturer in Aerospace Engineering, University of Bristol, brano.titurus@bristol.ac.uk

Figure 1: ERICA tiltrotor concept

A lack of nonlinear analysis in the design of larger tiltrotor aircraft could be a significant liability. Additionally, the continual development of technology means that the new, larger tiltrotors will likely utilise newer, lighter materials and rotor systems with different per-rev frequencies, pushing the prediction of coupling between destabilising modes outside existing knowledge[2].

The aim of this study is to achieve a broad picture of whirl flutter models and their associated stability analysis methods, with an aim to understand what models and analysis methods constitute the best approach for designing larger future tiltrotors in the context of whirl flutter stability.

Models and stability methods

W. H. Reed[3] originally derived simple linear whirl flutter models to understand the basic interactions. With the increase of computational power, models increased in complexity, and today's models use CAMRAD or similar software to analyse wing and rotor dynamics together.

Eigenvalue analysis is used to assess the stability of linear systems, and continuation and bifurcation methods can be used for nonlinear systems. Time simulations can be used in both cases to corroborate calculated findings.

Numerical continuation and bifurcation techniques calculate the steady-state solutions of a dynamical system as one of its parameters, called the continuation parameter, is varied[4]. The computed solutions construct a number of branches that can be either stable or unstable. To determine their stability, either an eigenvalue or Floquet analysis is carried out at each computed solution point, depending on the nature of the solution. For behaviours considered to be in equilibrium (fixed points), an eigenvalue analysis can be used (requiring local linearization in the case of a nonlinear system), whereas periodic behaviours (limit cycles) require Floquet theory to determine the stability[5].

Results and conclusions

A range of whirl flutter models and stability analysis methods are explored and their relative merits and drawbacks are discussed, with the aim of developing an approach or set of approaches that is most suitable for the design of the type of large tiltrotor required for the solution of the air traffic congestion problem. The impact and consequential importance of the modelling of system nonlinearities is also demonstrated.

References:

[1] Acree C. W., Johnson W., Aeroelastic Stability of the LCTR2 Civil Tiltrotor, 2008
[2] Ibid.
[3] Reed W. H., Propeller-Rotor Whirl Flutter: A State-of-the-Art Review, 1965
[4] Rezgui D., Lowenberg M. H., On the nonlinear dynamics of a rotor in autorotation: a combined experimental and numerical approach, 2015
[5] Kuchment P. A., Floquet Theory for Partial Differential Equations, 1993

UK VERTICAL LIFT NETWORK

Annual Technical Workshop
“Taking a Snapshot of the Academic Research in Vertical Lift”,
22-23 May 2017.

Aeroacoustic Analysis of Modern Propeller Designs

Giulia Chirico *, George N. Barakos † and Nicholas Bown‡

The main target of aviation industry and research is to develop aircraft with low environmental impact, as regards both reduction in fuel burnt and acoustic emissions. In terms of fuel efficiency, propeller-driven aircraft are the best choice for short and medium range flights; however, their acoustic emissions are nowadays still higher than those required from future noise certifications[1, 2, 3]. Continuing Dowty Propellers’s IMPACTA project, this work intends to analyst propeller noise, aiming for a reduction and/or a modification of the acoustic spectra generated by the whole propulsion system of a turboprop aircraft.
Computational Fluid Dynamic (CFD) is used to study the acoustic features of a modern propeller design, as well as to estimate noise levels. The research considers the propeller both in isolated and installed configurations, allowing to investigate the physics of the propeller-airframe interaction and to quantify propeller installation effects. The availability of experimentally obtained Transfer Functions (TF) for a Fokker 50 aircraft also enables the evaluation of interior cabin noise. Furthermore, different blade and hub designs are compared in the work, in terms of overall Sound Pressure Level (SPL) and sound spectra characteristics, as well as preference judgements via encoded audio files.

The CFD solver HMB3 of Glasgow University[4, 5] has been first validated for propeller flows for both isolated and installed configurations, using the JORP[6] and the IMPACTA[7] experimental datasets respectively. The JORP is a single row six bladed propeller mounted on a minimum interference spinner, and measurements allows an evaluation of the computed blade pressure distribution[8]. The IMPACTA wind tunnel model is a scaled model of an installed turboprop

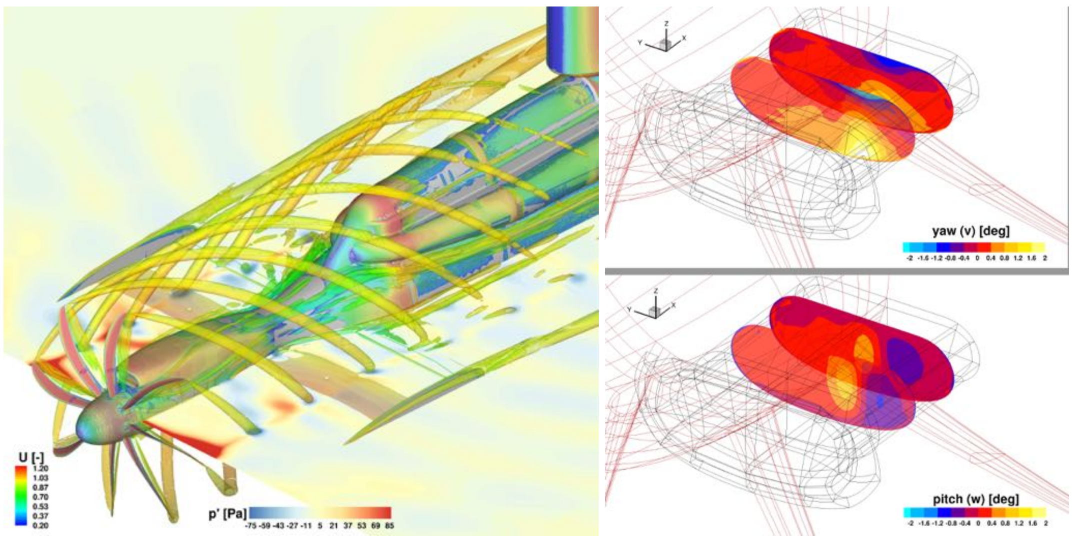

(a) Wake (iso-surface of *Q criterium* colored by adimensional axial velocity) and acoustic pressure field visualization.

(b) Visualization of the instantaneous flow distortion inside the engine intake.

Figure 1: IMPACTA Baseline wind tunnel scaled model (1:4.83) at cruise conditions ($M_\infty = 0.5$, $M_{TIP} \sim 0.63$). HMB3 URANS $k - \omega$ SST results of fine mesh.

power-plant, comprising propeller, nacelle, intake, and part of the wing. The IMPACTA propeller is a eight bladed propeller with extremely low activity factor, designed to operate at $M_\infty = 0.5$ and ~ 850 RPM at high blade loading conditions. Steady and unsteady pressure sensors enable a comparison of HMB3 predictions regarding aerodynamics and acoustics on the wing. In addition, mass flow rate and pressure measurements have been used to set up the boundary conditions of

*PhD Student - g.chirico.1@research.gla.ac.uk - CFD Laboratory, School of Engineering, University of Glasgow, G12 8QQ, UK
†Professor - George.Barakos@glasgow.ac.uk - CFD Laboratory, School of Engineering, University of Glasgow, G12 8QQ, UK
‡Project Engineer - Nicholas.Bown@dowty.com - Dowty Propellers, Anson Business Park Cheltenham Road East, Gloucester, GL2 9QN, UK

the intake face in the CFD simulation to represent the realistic suction conditions due to the engine. Some results for the IMPACTA wind tunnel case are reported, as example, in Figures 1 and 2. Overall, a fairly good agreement is registered. Finally, by comparison with the experimental data, the importance of the grid resolution is also pointed out. It is shown that,

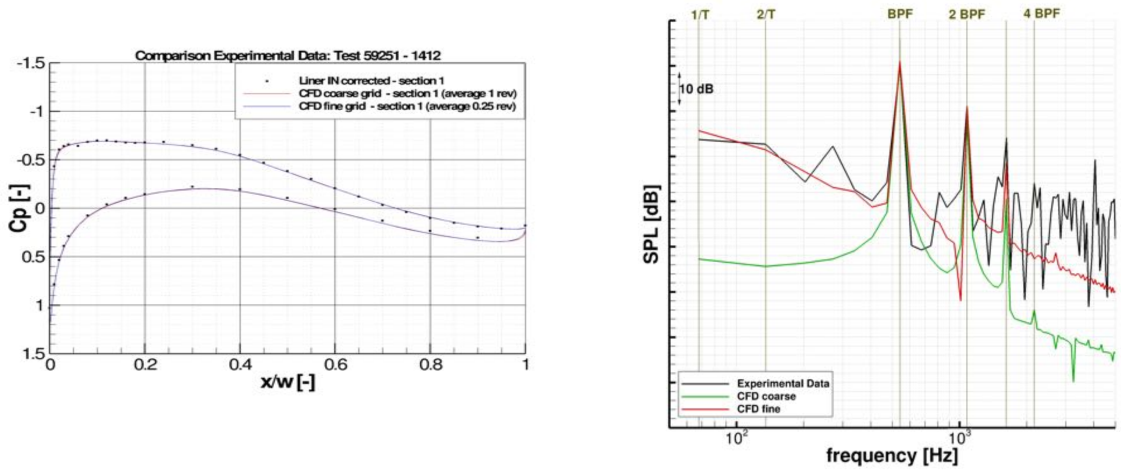

(a) Chord-wise pressure coefficient distribution on the wing: averaged CFD results *vs* steady pressure taps data. Span-wise section on the port wing, at 90% of the propeller radius.

(b) SPL spectra: numerical results of HMB3 *vs* Kulite measurements for one propeller revolution. Sensor on the port lower wing, at 92% of the propeller radius on the wing span and at 5% on the chord.

Figure 2: HMB3 validation: IMPACTA Baseline wind tunnel scaled model (1:4.83) at cruise conditions ($M_\infty = 0.5$, $M_{TIP} \sim 0.63$). Comparison between CFD results and experiments carried out by ARA[7].

regarding aerodynamic loads, the coarse grid ($\sim 20.1M$ cells) gives accurate prediction, while, regarding acoustics, the fine mesh ($\sim 161.3M$ cells, i.e. double spacial resolution in all directions) is needed to capture up to the third harmonic within 3 dB.

A complete aircraft with the Baseline IMPACTA propeller is simulated to analyze an installed configuration at full scale. A typical large twin-engined high-wing turboprop commercial airplane is considered, similar to the Fokker 50. Computational geometry and surface mesh are shown in Figure 3(a). A fully-matched structured multi-block grid is built around

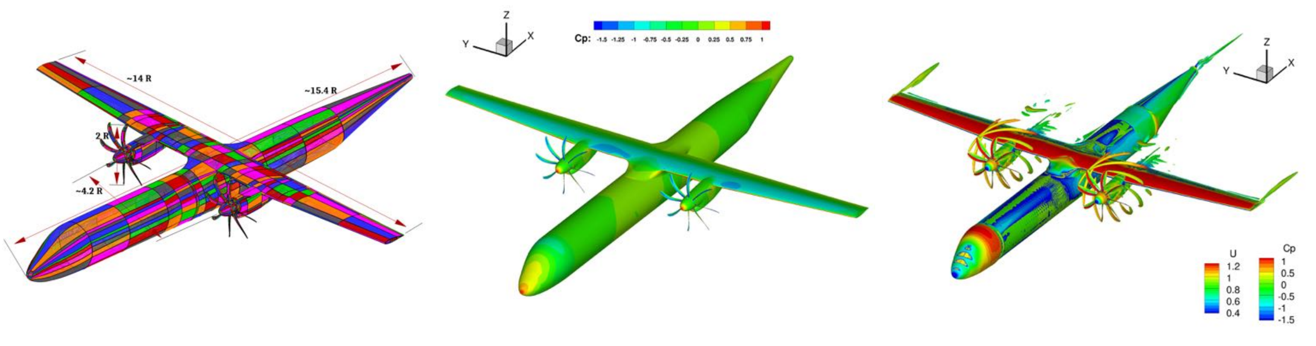

(a) Computational geometry. Dimensions reported as function of the full scale propeller radius R.

(b) HMB3 URANS $k-\omega$ SST results: pressure coefficient distribution on the aircraft after 1 propeller revolution.

(c) HMB3 URANS $k-\omega$ SST results: wake visualization via *Q criterium* iso-surfaces after 1 propeller revolution.

Figure 3: High-wing twin-engined turboprop aircraft with co-rotating propellers at cruise conditions. The conventional configuration with propellers rotating clock-wise when viewed from the rear has been chosen.

the aircraft, being especially careful to have a good quality mesh in areas which have proved critical in preliminary tests performed on half of the plane (e.g. fuselage-wing junction). The sliding plane technique[9] is employed to allow the relative motion and to exchange information between aircraft and propeller meshes, while the chimera overset method[10] is used to immerse the aircraft grid in a Cartesian background grid which is extended until the far-field where free-stream boundary conditions are applied. URANS (Unsteady Reynolds Averaged Navier-Stokes), closed by the $k-\omega$ SST turbulence model, are performed with HMB3 for the case of co-rotating propellers at cruise conditions, as it is the case of the majority of civil turboprops. Preliminary results are reported in Figures 3(b) and 3(c).

The isolated propeller tonal acoustics is analyzed through RANS computations of a single blade mounted on an infinite-long spinner, assuming the resulting flow-field is periodic both in space and time. To estimate the SPL, the equivalent unsteady pressure signal is reconstructed from the CFD solution after the convergence of the steady simulation. The acoustic analysis is performed considering an array of 32 by 33 points arranged on a half-cylinder, thus to mimic the fuselage of a fictitious high-wing aircraft and be able to compare the results with the installed test case. The correspondent interior cabin noise is finally evaluated by means of the application of the set of TF measured by NLR[11]. It is found that, due to the characteristics of the transmission loss, the pressure fluctuation magnitude is significantly reduced passing through the fuselage structure and that the main contribute to the interior sound signal is due only to the tone at the Blade Passing Frequency (BPF). As example, in Figure 4 are presented the instantaneous pressure distribution on the fictitious fuselage for

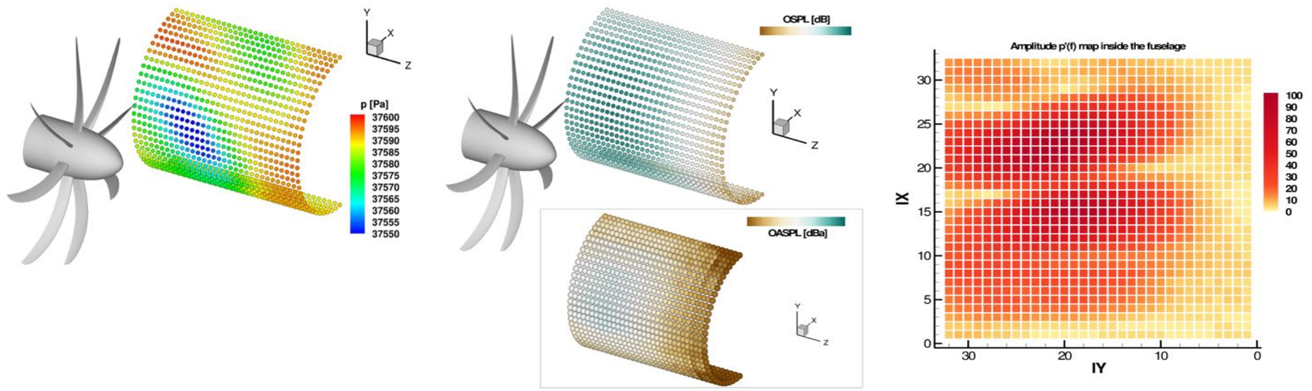

(a) Instantaneous pressure distribution on the exterior of the fictitious fuselage considered.

(b) Overall SPL and A-weighted value on the exterior of the fictitious fuselage considered.

(c) Adimensional acoustic pressure amplitude map on the interior of the fictitious fuselage using the TF of the Fokker 50 aircraft.

Figure 4: Isolated propeller at cruise conditions, RANS results, showing external and internal noise.

the Baseline IMPACTA propeller at cruise conditions, the correspondent overall SPL and the acoustic pressure amplitude map inside the aircraft cabin.
Single-blade RANS are also used to assess three different design solutions in addition to the Baseline IMPACTA propeller: *(i)* an Offloaded-Tip blade, *(ii)* a Staggered hub, *(iii)* an Unequally-Spaced hub. The Offloaded-Tip design is shown to be significantly quieter because of the lower operating RPM, due to the higher pitch, and the load moved inboard; however, a small performance penalty is found. The modified hub designs exhibit a modulation of the noise spectra as a consequence of the different geometric periodicities imposed, and only very slightly louder noise levels are registered. Their more continuous spectra should be more pleasant for the human ear; however, inside the fuselage, the differences in the spectra content, still visible and mainly due to the frequency at BPF/2, seems to not be perceived by the majority of the passengers because of the large reduction in the amplitudes.

Future developments of this research address to investigate the best option of propellers installation on the aircraft. Synchrophasing of the two propellers will be evaluated for the case of co-rotating propellers, as well as the effect of their rotational direction. A counter-rotating configuration, typical of military turboprops, will be also studied.
Regarding the CFD method, future work will focus, on one hand, on the evaluation of CFD techniques with lower turbulent viscosity than URANS (e.g. SAS[12] and DES[13]) with the aim to capture, at least in part, also the broadband noise content; on the other hand, on the evaluation of the HMB3 high-order scheme[14] performance.

Acknowledgements

This research is supported by Dowty Propellers[15]. Results were obtained using the EPSRC funded ARCHIE-WeSt High Performance Computer (www.archie-west.ac.uk), that is gratefully acknowledged for the time allocated. The authors would also like to thank ARA and NLR for the use of the experimental data.

References

[1] Pedro Argüelles, Manfred Bischoff, Philippe Busquin, BAC Droste, Sir Richard Evans, W Kröll, JL Lagardere, A Lina, J Lumsden, D Ranque, et al. European Aeronautics: a Vision for 2020 - Meeting Society's Needs and Winning Global Leadership. *Advisory Council for Aeronautics Research in Europe, Report*, 2001. URL `http://www.acare4europe.org/sites/acare4europe.org/files/document/Vision%202020_0.pdf`. Last vist: 04/01/2017.

[2] ACARE Strategy Review Group: A. Garcia, B. Bettignies-Thiébaux, P. Chivers, P. ande Desvallée, A. Junior, R. Kingcombe, M. Laroche, C. Latella, J. Martin-Hernandez, U. Moeller, N. Pilon, I. Ritchey, S. Side, and D. Young. ACARE -Aeronautics and Air Transport: Beyond Vision 2020 (Towards 2050). Technical report, European Commission, Directorate General for Research, Directorate H - Transport, Unit H.3 - Aeronautics, 2010.

[3] The High Level Group on Aviation Research: M. Darecki, C. Edelstenne, T. Enders, E. Fernandez, P. Hartman, J.-P. Herteman, M. Kerkloh, I. King, P. Ky, M. Mathieu, G. Orsi, G. Schotman, C. Smith, and J.-D. Wörner. Flightpath 2050: Europe's vision for aviation. *Report of the High Level Group on Aviation Research, Publications Office of the European Union, Luxembourg*, 2011. URL `http://ec.europa.eu/transport/sites/transport/files/modes/air/doc/flightpath2050.pdf`. Last vist: 04/01/2017.

[4] G.N. Barakos, R. Steijl, K. Badcock, and A. Brocklehurst. Development of CFD Capability for Full Helicopter Engineering Analysis. *31th European Rotorcraft Forum, Florence, Italy, Sept*, 2005.

[5] R. Steijl, G. Barakos, and K. Badcock. A Framework for CFD Analysis of Helicopter Rotors in Hover and Forward Flight. *International Journal for Numerical Methods in Fluids*, 51(8):819–847, 2006. doi: 10.1002/fld.1086.

[6] N. Scrase and M. Maina. The evaluation of propeller aero-acoustic design methods by means of scaled-model testing employing pressure tapped blades and spinner. In *ICAS PROCEEDINGS*, volume 19, pages 183–183. AMERICAN INST OF AERONAUTICS AND ASTRONAUTICS, 1994.

[7] A. Gomariz-Sancha, M. Maina, and A. J. Peace. Analysis of Propeller-Airframe Interaction Effects through a Combined Numerical Simulation and Wind-Tunnel Testing Approach. *AIAA SciTech, 53rd AIAA Aerospace Sciences Meeting, Kissimmee, Florida*, page 1026, 2015. doi: doi:10.2514/6.2015-1026.

[8] G.N. Barakos and C.S. Johnson. Acoustic comparison of propellers. *International Journal of Aeroacoustics*, 15(6-7): 575–594, 2016. doi: https://doi.org/10.1177/1475472X16659214.

[9] R. Steijl and G. Barakos. Sliding Mesh Algorithm for CFD Analysis of Helicopter Rotor˘Fuselage Aerodynamics. *International Journal for Numerical Methods in Fluids*, 58:527–549, 2008. doi: 10.1002/fld.1757.

[10] M. Jarwowsky, M.A. Woodgate, G. Barakos, and J. Rokicki. Towards Consistent Hybrid Overset Mesh Methods for Rotorcraft CFD. *International Journal for Numerical Methods in Fluids*, 74:543–576, 2014.

[11] E.G.M. Geurts. IMPACTA Transmission functions generation - test and processing. Technical Report NLR-CR-2013-145, National Aerospace Laboratory NLR, 2013.

[12] F. R. Menter and Y. Egorov. A Scale Adaptive Simulation Model using Two-Equation Models. *43rd AIAA Aerospace Sciences Meeting and Exhibit*, 2005. doi: http://dx.doi.org/10.2514/6.2005-1095.

[13] Michael L Shur, Philippe R Spalart, and Michael K Strelets. Jet noise computation based on enhanced des formulations accelerating the rans-to-les transition in free shear layers. *International Journal of Aeroacoustics*, 15(6-7):595–613, 2016. doi: https://doi.org/10.1177/1475472X16659388.

[14] A. Jimenez Garcia and G. N. Barakos. Implementation of high-order methods in the hmb cfd solver. In *73rd AHS International's Annual Forum and Technology Display*, 2017.

[15] Dowty Aerospace Propellers. `http://dowty.com`. Last Visit: 11/09/2015.

Counter Rotating Open Rotors for General Aviation

Dale Smith, Antonio Filippone
University of Manchester

Civil aviation accounts for 2% of the worlds CO_2 emission [1], this equated to around 700 million metric tonnes in 2013, and is set to treble by 2050[2]. These worrying levels of emissions cannot be ignored, and as a result the EU has set very demanding emission targets for manufacturers to meet before the year 2050[3][4]. In an effort to meet these targets, Counter Rotating Open Rotor (CROR) technology has been the subject of renewed interest, this, due to its promise of up to a 25% reduction in fuel consumption [5]. As well as this, use of CROR eliminates the need for torque reaction as is necessary with single rotation propellers. However, these gains come at the cost of greater noise and greater mechanical complexity. Most recent work on CROR technology has focussed on addressing the issues over noise. However, there remains little published data surrounding the aerodynamics of CROR's and the mechanical issues associated with CROR technology. This work will present an initial investigation into the aerodynamics of CROR's, supported by an aerodynamic optimisation of CROR geometry. As well as this, work carried out on turboelectric propulsion, a potential technology that may help over come the mechanical complexities associated with CROR, will be presented.

A low order Blade Element Momentum Theory (BEMT), model has been employed to perform a preliminary investigation of CROR aerodynamics. The BEMT model used the annular form of the general momentum theory in order to allow the induced velocities to take their own form. The model considered two propellers in isolation and coupled them by means of mutually induced velocities, thus accounting for the interference and interactions between the two rotors. These mutually induced velocities are related to the self induced velocities by a constant that is dependant on the axial spacing between rotors, and their precise form developed on physical reasoning. These mutually induced velocities are, like the self induced velocities, used to update the velocity triangles and hence the BEMT calculations Figure1 shows the velocity triangles for the CROR blade pair. The BEMT model allowed initial investigation of the CROR

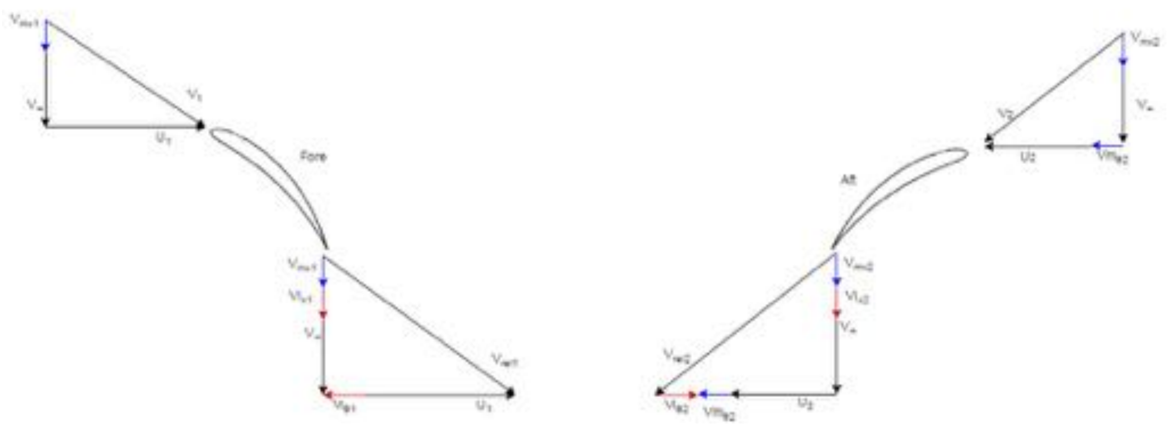

Figure 1: Velocity triangle components for CROR

aerodynamics at extremely short computation times. Currently, the model uses data for the SC1095 aerofoil (by means of a look up table)[6], and this gives rise to some of the current limitations of the model, e.g. there is no account for blade camber of thickness. It is hoped to implement a model to calculate aerofoil properties within the BEMT model and hence account for all geometric properties of the propeller blades. Nonetheless, the model accounts for all other geometric parameters of the blade, e.g. sweep, twist, etc. The model has been used to show the efficiency gains over a single rotation propeller and to investigate the performance of CROR's for various geometries.

Currently the BEMT model is being couple to a Genetic Algorithm (GA) optimiser. Due to the low computational time of the BEMT model, the optimiser can produce aerodynamically optimal geometries over a relatively short period of time. The GA is based on Darwinian evolutionary theories to produce successive generations of improved solutions. The optimisation is being performed to maximise efficiency whilst meeting a specified power requirement. As a purely aerodynamic optimisation, one has to give great consideration to the geometries produced. For example, interactions between the fore tip vortices and the aft rotor are a major source of noise and hence the aft blade is typically clipped. Clipping the aft blade gives reduction in aerodynamic efficiency as the clipped portion of the aft rotor cannot counteract the swirl imparted by the fore blade tip sections. Therefore, the optimiser would give an optimal solution for zero clipping. As such, clipping was set to 10% and removed from the optimisation. As well as acoustic consideration, one must give structural considerations. It is important to ensure the geometries produced are real and physically possible. Therefore, radially varying geometric parameters were parametrised using a class/shape function method[7]. This method gives smooth well behaved functions representing blade geometry. Parametrisation also significantly reduces the number of design variables within the optimisation routine and hence reducing computation time. The optimisation is being carried out for a general aviation aircraft in cruise, with the objective of maximum efficiency whilst meeting a given power requirement.

As mentioned, implementation of CROR technology comes with inherent mechanical complexities, requiring the use of multiple gears to deliver the counter rotation and thus generating greater mechanical losses, vibrations, etc. Work has been carried out in investigation of turboelectric propulsion technology to overcome these mechanical complexities. Turboelectric propulsion couples the mechanical engine (gas turbine, diesel etc), to an electric motor to deliver hybrid power to the propeller drive shaft. Coupling the mechanical engine with two electrical motors can over come the inherent mechanical complexities with using gearboxes to deliver the counter rotation. Figure 2 presents the layout of the turboelectric system. The use of electric

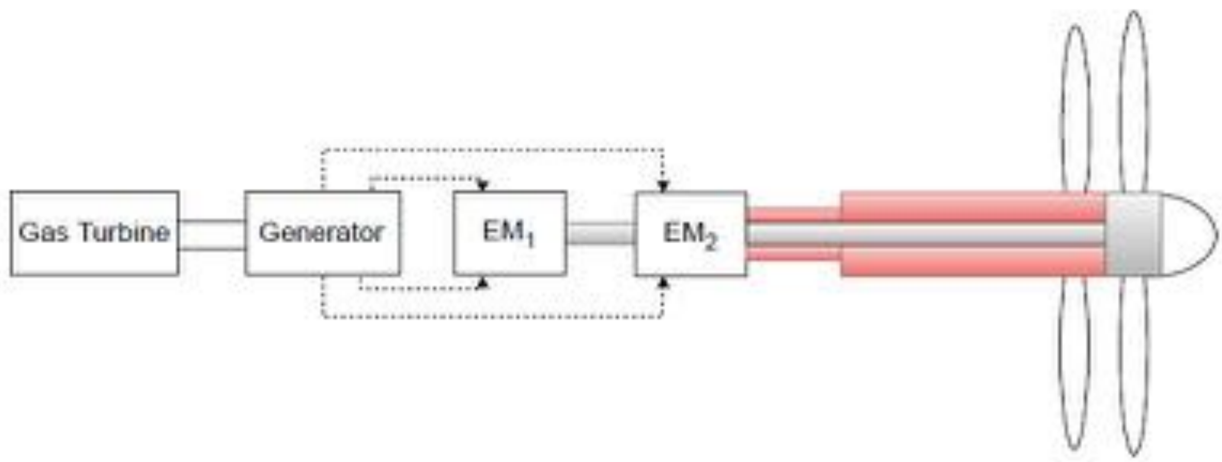

Figure 2: Use of turboelectric technology for CROR propulsion

motors to deliver torque to CROR has been proven for electric only aircraft (e.g see [8, 9]), and the use of turboelectric aircraft is currently an area of significant interest[10, 11, 12], as a means of cutting aircraft emissions to meet the targets discussed above. However, certain challenges arise when employing turboelectric technology. The most significant being the required increase in structural mass. Both motors have to be sized to deliver the full power of each propeller, this leading to a significant increase in structural mass. Despite this, future motor technology promises to deliver much greater specific energies, e.g. HTS motors. Another challenge arises if batteries are to be used to increase hybridisation in an attempt to further reduce emissions. Again if the required power share is too great, battery mass very quickly becomes excessive, making their use infeasible. Preliminary work on the feasibility of turboelectric propulsion for a general aviation aircraft with a propeller of single rotation, found it to be infeasible with the current state of the art of technology. However, it was found that the promisd improvements in battery technology (e.g commercialisation of LI-S and Li-Air batteries), offered the greatest potential for its feasibility. Nonetheless, if these challenges can be overcome, the benefits of using a turbolelctric propulsion for CROR technology will become feasible and further benefit the case for the use CROR propulsion.

This work has presented the preliminary investigation of CROR aerodynamics using a low order BEMT model. The optimisation should produce aerodynamically optimised results for maximum efficiency for a given power requirement. Upon generation of the optimised design, CFD work will be carried out to further investigate the aerodynamics of CROR's, specifically rotor-rotor interactions. These findings will then be used to strengthen the low order BEMT model. Work has also been presented on the investigation of the feasibility of turboelectric propulsion. It was found to be infeasible with the current state of the art, however, future battery and motor technologies will see the feasibility of turboelectric aircraft and remove the inherent mechanical complexities associated with CROR.

References

[1] W. Cao, B. C. Mecrow, G. J. Atkinson, J. W. Bennet, and D. J. Atkinson, "Overview of Electric Motor Technologies Used for More Electric Aircraft (MEA)," *IEEE Transactions on Industrial Electronics*, vol. 59, no. 9, pp. 3523–3531, 2012. [Online]. Available: http://ieeexplore.ieee.org/xpls/abs_all.jsp?arnumber=5991952

[2] C. Nunez, "Airplanes Next in Line for Carbon Rules?" 2015. [Online]. Available: http://news.nationalgeographic.com/energy/2015/04/150409-epa-aviation-emissions-rules-for-airplanes/

[3] ACARE, "Strategic Research & Innovation Agenda," vol. 1, 2012. [Online]. Available: http://www.eurosfaire.prd.fr/7pc/doc/1349425601_sria_acare_vol1.pdf

[4] European Comission, "Flightpath 2050 Europe's Vision for Aviation," *Report of the High Level Group on Aviation Research*, p. 28, 2011. [Online]. Available: http://ec.europa.eu/transport/modes/air/doc/flightpath2050.pdf

[5] P. Schimming, "Counter rotating fans An aircraft propulsion for the future?" *Journal of Thermal Science*, vol. 12, no. 2, pp. 97–103, 2003. [Online]. Available: http://dx.doi.org/10.1007/s11630-003-0049-1

[6] A. Filippone, "Rapid Estimation of Airfoil Aerodynamics for Helicopter Rotors," *Journal of Aircraft*, vol. 45, no. 4, pp. 1468–1472, 2008. [Online]. Available: http://arc.aiaa.org/doi/abs/10.2514/1.35560

[7] B. M. Kulfan, "Universal Parametric Geometry Representation Method," *Journal of Aircraft*, vol. 45, no. 1, pp. 142–158, 2008. [Online]. Available: http://dx.doi.org/10.2514/1.29958

[8] Electroflight LTD, "Electro-Flight." [Online]. Available: http://www.electro-flight.com/

[9] ContraElectric Propulsion LTD, "Contra Electric Propulsion Ltd — THE ADVANTAGES OF ELECTRIC CONTRA ROTATION." [Online]. Available: http://www.contraelectric.com/innovation/the-advantages-of-electric-contra-rotation

[10] K. P. Duffy, "Electric and Turboelectric Propulsion," *AIAA Propulsion and Energy Conference*, pp. 1–10, 2015.

[11] J. L. Felder, H. D. Kim, and G. V. Brown, "Turboelectric Distributed Propulsion Engine Cycle Analysis for Hybrid-Wing-Body Aircraft," *47th AIAA Aerospace Sciences Meeting including the New Horizons Forum and Aerospace Exposition*, no. January, pp. AIAA 2009–1132, 2009. [Online]. Available: http://dx.doi.org/10.2514/6.2009-1132

[12] M. Hepperle, "Electric FlightPotential and Limitations," 2012. [Online]. Available: http://core.kmi.open.ac.uk/download/pdf/11153363.pdf

Noise Control for a Trailing-edge Serrated Aifroil in Tandem Configuration

Xiao Liu[1], Syamir Alihan Showkat Ali[2] and Mahdi Azarpeyvand.[3]
University of Bristol, Bristol, United Kingdom, BS8 1IR

ABSTRCAT- This paper presents a comprehensive study on the application of serrations as a passive control method for reducing the aerodynamic sound from airfoils in tandem. The aim of the study is to investigate the efficiency of serrated trailing edge on cambered NACA 65-710 tandem airfoils to control and regularize the turbulence flow within the gap between the two airfoils (see Fig1). The effects of serrated trailing edges have been assessed using the rear airfoil which is equipped with several pressure taps and surface pressure transducers. Different types of serrations were tested in this experiment. The wake profiles have been quantified using two-dimensional Particle Image Velocimetry (PIV). Results show that the use of serrations do not have large effects on the wake development and the TKE at small angles of attack (0^o-5^o). However, at relatively high angles of attack, where maximum lift-to-drag can be obtained (10^o-15^o) the results show that significant reduction of turbulence kinetic energy and shear stress can be obtained (see Fig 2), which is believed to be due to the interaction between the flow field over the tip and root planes of the serrations. Preliminary results on the use of serrations confirmed that the serrated trailing edge can lead to robust control of the flow, and hence regulating the aerodynamic sound generation mechanism. In order to further demonstrate the effectiveness of serration treatment for reducing aerodynamic noise, the surface pressure fluctuations measurements have been conducted using the remote sensing method on the rear airfoil. It can be seen that the pressure fluctuations of the serrated cases show less changes at low angle of attack (0^o-5^o), while at relatively higher angles (10^o-15^o), it can be seen that the pressure fluctuations of the serrated cases on the suction side with gap between front and rear airfoils of W=1.0c for all the measured locations are relatively low for $fc/U_0 < 10$, while no changes in φ_{pp} is seen between the serrated and baseline case at $f\,c/U_0 > 10$ (See Fig 3).

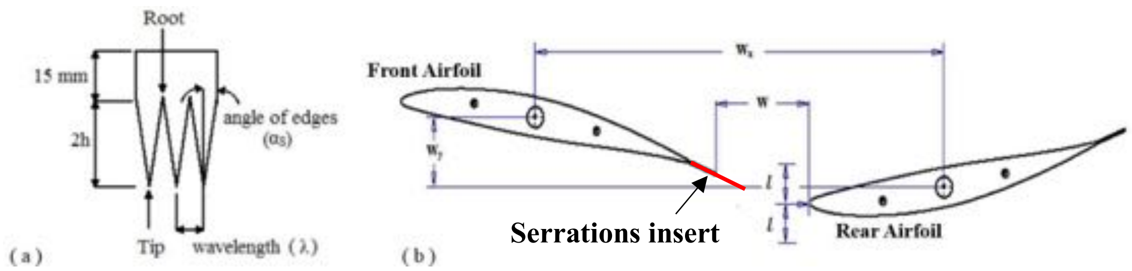

Fig. 1 (a) Tandem airfoils setup (b) Trailing-edge treatment: Sawtooth serration

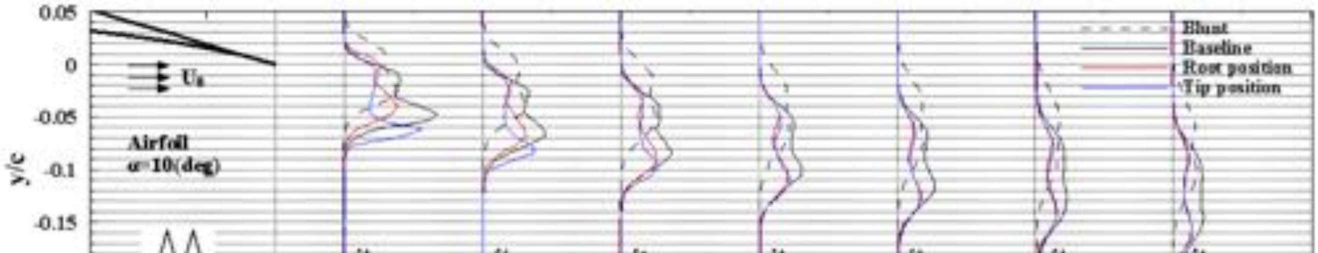

Fig. 2 Wake TKE profile for serrated NACA 65-710 airfoil at AoA=10^o and U_0=30 m/s. Black line: baseline; Red line: root location; Red line: tip location

[1] PhD Student, Department of Mechanical Engineering, xiao.liu@bristol.ac.uk.
[2] PhD Student, Department of Mechanical Engineering, ss14494@bristol.ac.uk.
[3] Senior Lecturer and Royal Academy of Engineering research fellow, Department of Mechanical Engineering, m.azarpeyvand@bristol.ac.uk.

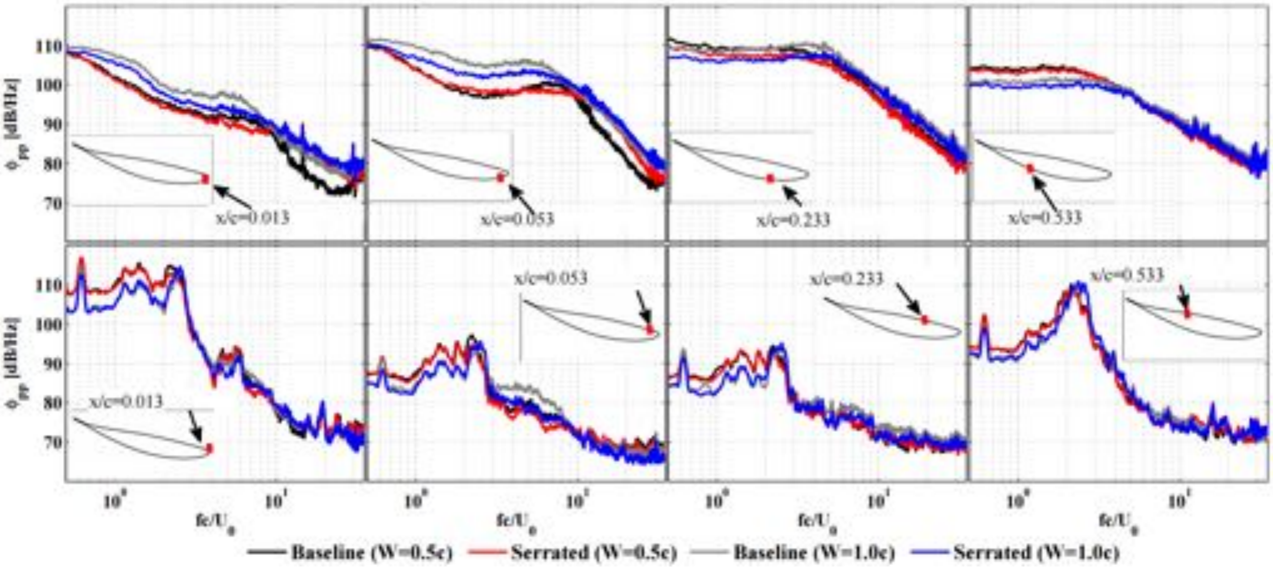

Fig. 3 Surface pressure fluctuations results for baseline and serrated NACA 65-710 airfoils at AoA=10^o , W = 0.5c and 1.0c at U_0=30 m/s.

Delay of dynamic stall using pulsed air jet vortex generators

R.B. Green[1], S.A. Prince[2], Y. Wang[1], V. Khodagolian[3], and F.N. Coton[1]

[1]Aerospace Sciences Division, University of Glasgow, UK
[2]School of Aerospace, Transport and Manufacturing, Cranfield University, UK
[3]Stockholm, Sweden

Abstract

Wind tunnel tests of an aerofoil section undergoing oscillatory and constant rate pitching were carried out to investigate how air jet vortex generators might be used to improve the performance of a helicopter main rotor aerofoil section for dynamic stall. Following results of earlier research, a single, spanwise array of jets was fitted to the 12% chord location of a RAE9645 aerofoil section. Surface mounted pressure transducers provided data during the dynamic stall process, and allowed the dynamic stall performance to be evaluated in terms of pitching moment excursion, cycle damping and normal force behaviour. Data analysis using the Hilbert transform has permitted an improved analysis of damping compared to the cycle damping coefficient. Pulsed blowing was found to be far more effective than steady blowing even at much reduced jet momentum coefficients, see figure 1. The primary effect of the jet blowing is the suppression of the dynamic stall to higher angle of attack, and in the cases where positive cycle damping was restored the dynamic stall only appeared in a highly attenuated form.

(a) steady blowing, C_n (b) pulsed blowing, C_n

(c) steady blowing, C_m (d) pulsed blowing, C_m

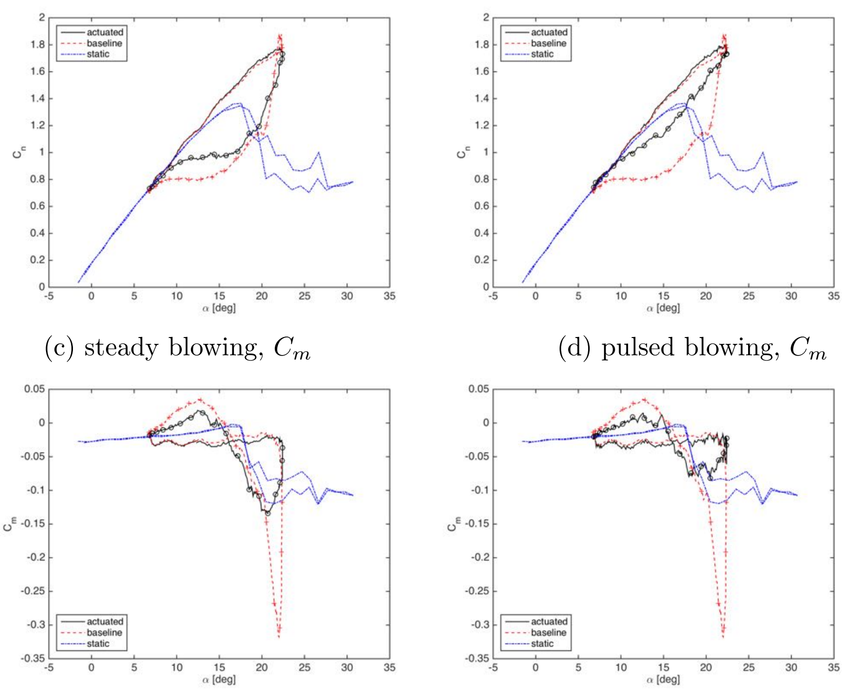

Figure 1: Normal force coefficient C_n and moment coefficient C_m cycles for reduced frequency k =0.103, pitch amplitude $\hat{\alpha} = 8^o$, mean angle $\bar{\alpha} = 14^o$. Frames (a) and (c) are for steady blowing test S317 at blowing coefficient $C_\mu = 0.0028$, frames (b) and (d) are for pulsed blowing test P332 at blowing coefficient $C_\mu = 0.0015$ (duty cycle blowing coefficient $C_{\mu D} = 0.00075$), pulsing reduced frequency $F^+ = 1.04$, 0.5 duty cycle. The symbols on the plots indicate the downstroke.

3rd UK Vertical Lift Network Annual Technical Workshop
22-23 May 2017, Pott Shrigley, Cheshire, UK

CFD Methods Development for the Simulation of Tilt Rotor Aircraft in the HiPerTilt Project

F. Dehaeze[1], C. B. Allen[2], G. N. Barakos[3]

1. Leonardo Helicopters
Yeovil BA20 2YB, UK
http://www.leonardocompany.com/

2. University of Bristol
Bristol BS8 1TR, UK
http://www.bristol.ac.uk/

3. University of Glasgow
Glasgow G12 8QQ, UK
http://www.glasgow.ac.uk/

Following the development of tilt rotor aircraft, a need for new adapted CFD methods arose. The HiPerTilt project aimed at developing new aerodynamics methods, tailored for industrial needs, with the participation of the Universities of Bristol and Glasgow, who are specialised in CFD simulations for rotorcraft. The HiPerTilt project focused on tilt rotor aircraft; however, the developed methods should also be compatible with the simulation of standard helicopters and new advanced configurations. The project was divided in two main parts, one dealing with the aircraft body's aerodynamics, the other one with the rotor aerodynamics.

The main goal of the aircraft body's aerodynamics work package was the improvement of the wing efficiency. Due to the specificities of tilt rotor aircraft, the wing has a highly constrained design, making any optimisation of its shape highly challenging. In cooperation with the University of Bristol, new aerofoil optimisation techniques were developed to be able to account for all constraints of a tilt rotor[1]. Another study by the University of Bristol focused on the vortex generators. Simulating the effect of vortex generators in CFD has a high cost, which is not compatible with optimisers, requiring a high number of simulations. Various vortex generator models were assessed, and the effect of the location, size and shape of the vortex generators was evaluated on infinite-span wings. These simulations are also used as a validation of various vortex generator models, which are then used on a finite-span wing[2]. A wind tunnel test was also performed to create an additional validation database for the new CFD models.

The rotor aerodynamics work, in collaboration with the University of Glasgow, focused on comparing and validating various methods for the prediction of tilt rotors in both hover and propeller mode[3]. Based on the method validation, a new approach to tilt rotor design based on the industrial requirements was developed. The University of Glasgow developed the HMB CFD solver, also in use at Leonardo Helicopters, to be able to simulate every flight phase, with the ability to also include the fuselage and wing in the simulations, highlighting the interference from the other parts[4]. The University of Glasgow also worked on acoustic methods to assess the noise emitted by both standard and tilt rotors.

The paper will describe in details the cooperation between the members of the HiPerTilt consortium. The technical and organisational challenges, arising from the cooperation between industrial and academic partners, will be highlighted as well as the approach used to go beyond these differences. Suggestions for future projects will also be given.

Acknowledgements
The financial support from Innovate UK for the HiPerTilt project is gratefully acknowledged

References:

[1] D.J. Poole, C.B. Allen, T. Rendall, Control Point-Based Aerodynamic Shape Optimization Applied to AIAA ADODG Test Cases, in *Proceedings of the 53rd AIAA Aerospace Sciences Meeting*, Kissimmee, Florida, 5-9 Jan. 2015, Paper AIAA 2015-1947.

[2] R. Bevan, D.J. Poole, C.B. Allen, T. Rendall, Simulation and Surrogate-Based Design of Rectangular Vortex Generators for Tiltrotor Aircraft Wings, in *Proceedings of the 33rd AIAA Applied Aerodynamics Conference*, Dallas, TX, 22-26 Jun. 2015, Paper AIAA 2015-2725.
[3] A. Jimenez-Garcia, G.N. Barakos, Hover Performance Predictions for the S-76 Main Rotor Blade, in *Proceedings of the 53rd AIAA Aerospace Sciences Meeting*, Kissimmee, Florida, 5-9 Jan. 2015, Paper AIAA 2015-1712
[4] A. Jimenez-Garcia, G.N. Barakos, CFD Simulations of the ERICA tiltrotor using HMB2, in *Proceedings of the 54th AIAA Aerospace Sciences Meeting*, San Diego, California, USA, 4-8 Jan. 2016, Paper AIAA 2016-0329.

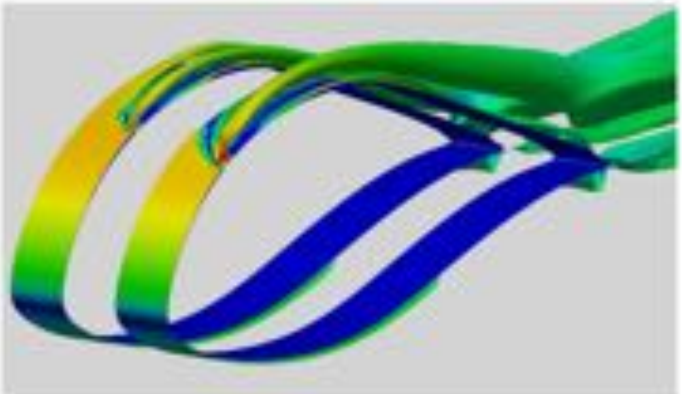

Figure 1: Simulation of two vortex generator configurations for a thick aerofoil, University of Bristol.

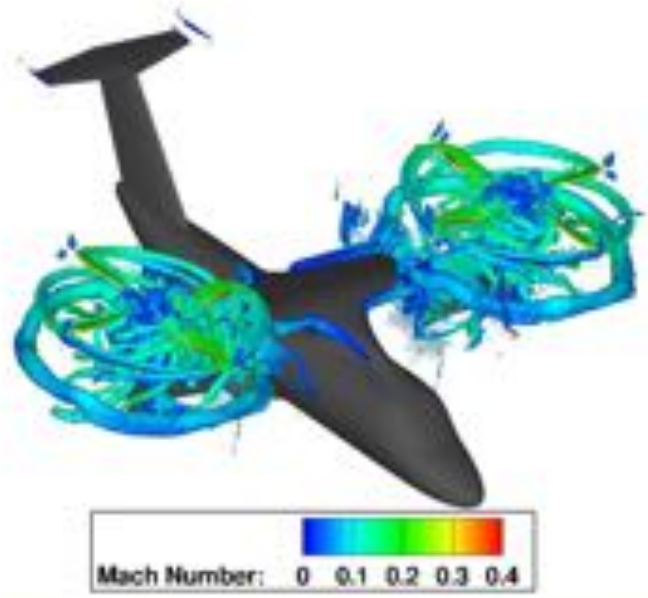

Figure 2: Simulation of a full tilt rotor aircraft in hover, University of Glasgow.

Heliflight-R Rotorcraft Simulator Fidelity Research

Wajih A. Memon and Mark D. White
Flight Science & Technology Research Group, School of Engineering,
The University of Liverpool, UK.

I. Introduction

Heliflight-R simulator at the University of Liverpool, Flight Simulation Laboratory is a reconfigurable research flight simulator, installed and commissioned in 2008 [1]. It consists of 12-ft visual dome mounted on 6-DOF Moog hexapod motion system. The simulator uses three high-resolution projectors, providing the horizontal and the vertical projection of 210° and 70°, respectively. The simulator is utilised for piloted rotorcraft simulations for undergraduate aerospace engineering projects and postgraduate research activities [1]. Quantification of fidelity of the rotorcraft simulators has been an important concern in the rotorcraft world due to its operations in different harsh environments, e.g civil and military services [2]. Attempts have been made to qualify the overall simulation fidelity for the rotorcraft simulators but only within the framework of flight handling qualities which serves the purpose partially [3, 4].

II. Motion Cueing and Tuning

Motion cueing in rotorcraft flight simulators has been an important point of concern for several years due to unavailability of standard guidelines, e.g. CS-FSTD (H) [5]. There is still a conflict regarding whether motion cue is a significant element of overall simulator fidelity and should be included in the simulation or it only acts as a cause for pilot sickness and false pilot perception. Research is being carried out currently on exploring ways of optimising motion fidelity in Heliflight-R (6-DOF) full motion simulator at Flight Simulation Laboratory, University of Liverpool (Fig.1) [1].

Fig. 1: Heliflight-R UoL Simulator

The rotorcraft simulation fidelity is based on three main elements; flight mechanics model based on FLIGHTLAB software, visual cueing from VEGA software, and motion cueing system (Fig.2). The current focus of the ongoing project is on structured examination of individual and combined significance and dependency of motion cueing as a single simulation element on the overall fidelity of the helicopter flight simulation for different tasks and in different environmental conditions (Fig.2). The analysis and assessment of objective motion fidelity and perceptual motion fidelity between a real helicopter and Heliflight-R simulator are considered for qualification of the motion system in the simulator.

Fig. 2: Rotorcraft Flight Simulation Fidelity Elements

The objective fidelity assessment consists of Objective Motion Cueing Test (OMCT) on the rotorcraft flight simulator to construct acceptable/uncertain/unacceptable fidelity boundaries to allow comparison with different motion tuning sets before flight trial. A simulated OMCT test is carried out using MatLab Simulink model of Heliflight-R simulator in which a sinusoidal signal stream of the discrete set of 12 frequencies ranging from 0.1-15 rad/sec of 5 periods is injected in the Motion Drive Algorithm (MDA), at the pilot position in the helicopter and accelerations at the pilot position in the simulator are measured (Fig.3), [6]. FFT of data is carried out to estimate the frequency analysis (bode plots) between the two datasets.

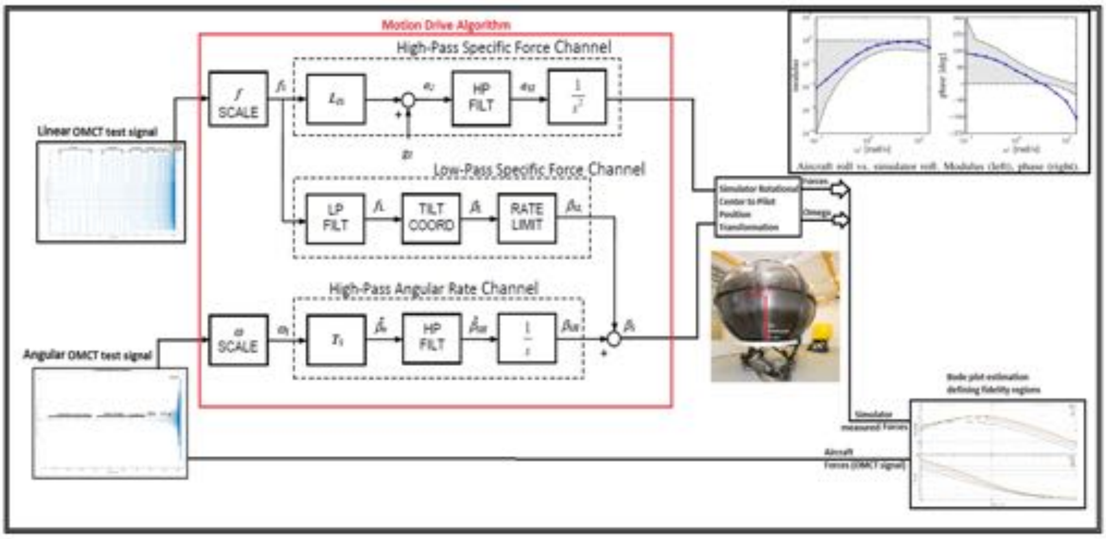

Fig. 3: OMCT Test Algorithm

Perceptual motion fidelity assessment consists of offline purpose based motion tuning technique of high-pass and low-pass filter parameters in classical washout algorithm (CWA). The tuning technique is based on the minimization of vestibular motion perception error (VMPE) between helicopter and simulator to serve the interest of similar motion cueing in the simulator as in a real helicopter (Fig.4).

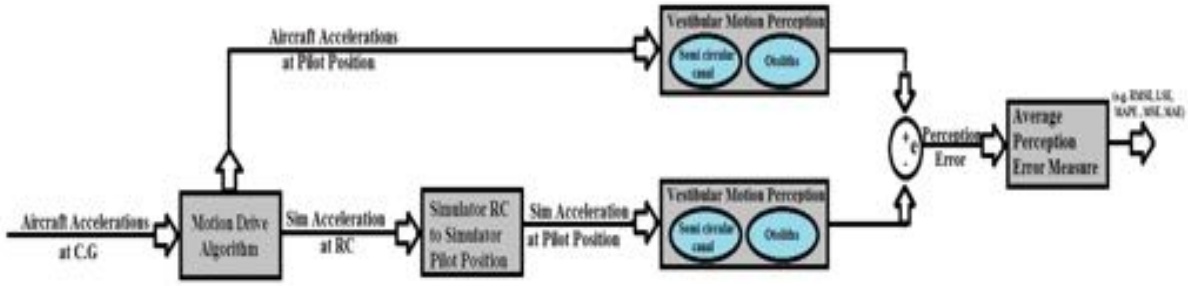

Fig. 4: Vestibular Motion Perception Error (VMPE) Tuning Technique

Simulink based model is constructed to simulate the accelerations at the pilot position in helicopter and simulator, efficient vestibular mathematical models are integrated with it to simulate the perceived accelerations. The perception data is compared to calculate the central tendency and dispersion measures as shown in (Table.1). Tuning of the MDA is suggested by varying the values of gains ‘k’ and washout frequencies ‘ω_n’ of the generic 3rd order MDA filters keeping the VMPE and Heliflight-R simulator excursion limits constrained. The simulated VMPE results are compared with existing subjective motion fidelity pilot ratings as shown in (Fig.5), for Pirouette Task contained within ADS 33 [7].

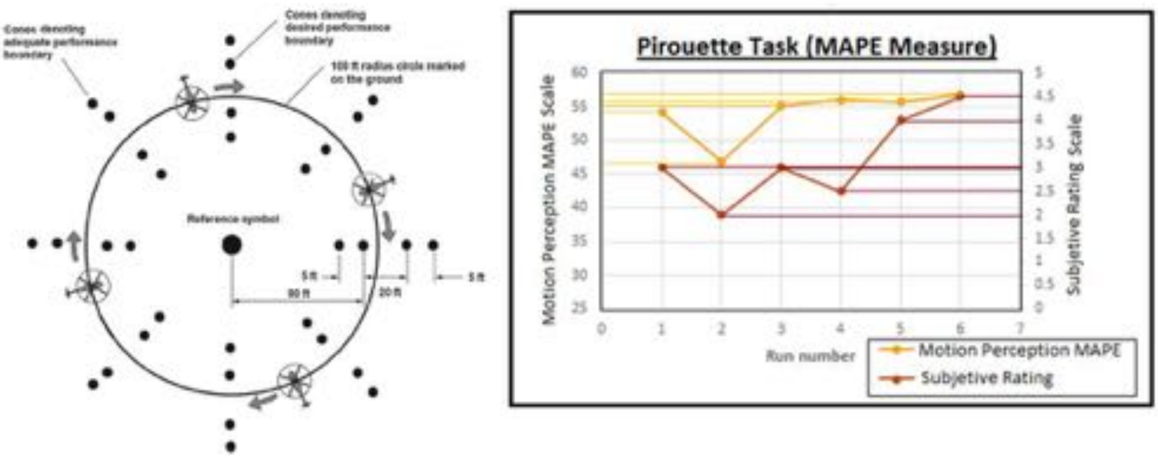

Fig. 5: Pirouette Task and Comparison of VMPE with Subjective Motion Fidelity Rating

Moreover, similar VMPE technique was used to tune the simulator platform response for the aggressive task. VMPE was compared for three motion tuning sets; Standard-heli (Responsive), Aerobatics (Benign) and Optimised (Minimised VMPE), using different measures (Table. 1). The correlation coefficient of helicopter and simulator angular accelerations for three motion sets are compared for demonstrating simulator response improvement (Fig.6 & 7).

Table 1: Central tendency and dispersion measures for three motion tuning sets

Standard-Heli

DoF	RMSE	MSE	LSE	Area	MAE	MPE	CCr
x	0.608411	0.370163	12410.47	15383.09	0.458827	45.8827	0.382861
y	1.189886	1.415829	47468.5	25662.85	0.765438	76.54383	0.278975
z	1.018929	1.038217	34808.29	9327.979	0.278223	27.82229	0.489153
p	0.039465	0.001557	52.21666	908.0434	0.027084	2.708394	0.516425
q	0.046974	0.002207	73.97895	987.4905	0.029454	2.945359	0.674662
r	0.047416	0.002248	75.37914	1194.555	0.03563	3.562965	0.501752
Avg	0.491847	0.471704	15814.81	8910.669	0.265776	26.57759	0.473971

Aerobatics

DoF	RMSE	MSE	LSE	Area	MAE	MPE	CCr
x	0.625641	0.391427	13123.36	15681.82	0.467737	46.77371	0.685981
y	1.211394	1.467476	49200.05	26049.9	0.776983	77.69828	0.228378
z	1.04572	1.093529	36662.76	9594.439	0.286171	28.61705	0.431787
p	0.041375	0.001712	57.3937	987.2801	0.029447	2.944731	0.367869
q	0.051025	0.002604	87.2881	1125.429	0.033568	3.356784	0.495912
r	0.050609	0.002561	85.87183	1267.59	0.037808	3.780804	0.203722
Avg	0.504294	0.493218	16536.12	9117.743	0.271952	27.19523	0.402275

Optimised

DoF	RMSE	MSE	LSE	Area	MAE	MPE	CCr
x	0.571652	0.326786	10956.17	14316.11	0.427002	42.70024	0.57794
y	1.168301	1.364928	45761.93	24761.91	0.738566	73.85661	0.426113
z	1.018917	1.038191	34807.44	9339.644	0.278571	27.85708	0.489157
p	0.037623	0.001415	47.45619	877.439	0.026171	2.617111	0.696627
q	0.044163	0.00195	65.39114	927.3685	0.02766	2.766035	0.72178
r	0.046396	0.002153	72.17117	1159.2	0.034575	3.457512	0.686499
Avg	0.481175	0.455904	15285.09	8563.611	0.255424	25.54243	0.599686

Measures

RMSE	Root Mean Square Error
MSE	Mean Square Error
LSE	Least Square Error
Area	Area between two perceptions
MAE	Mean Absolute Error
MPE	Mean Percentage Error
CCr	Cross Correlation

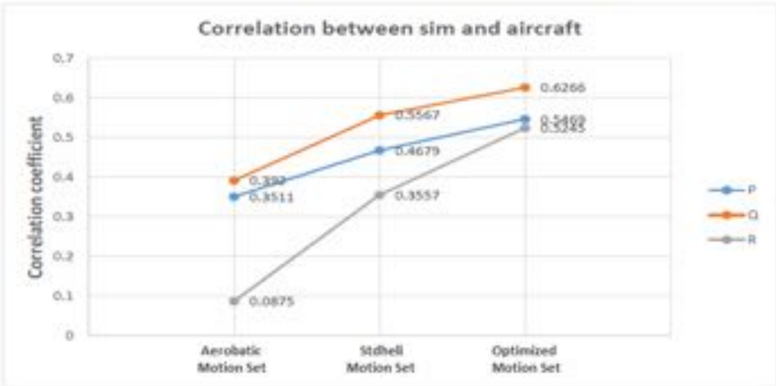

Fig. 6: Comparison of Correlation Coefficient of three motion tuning sets

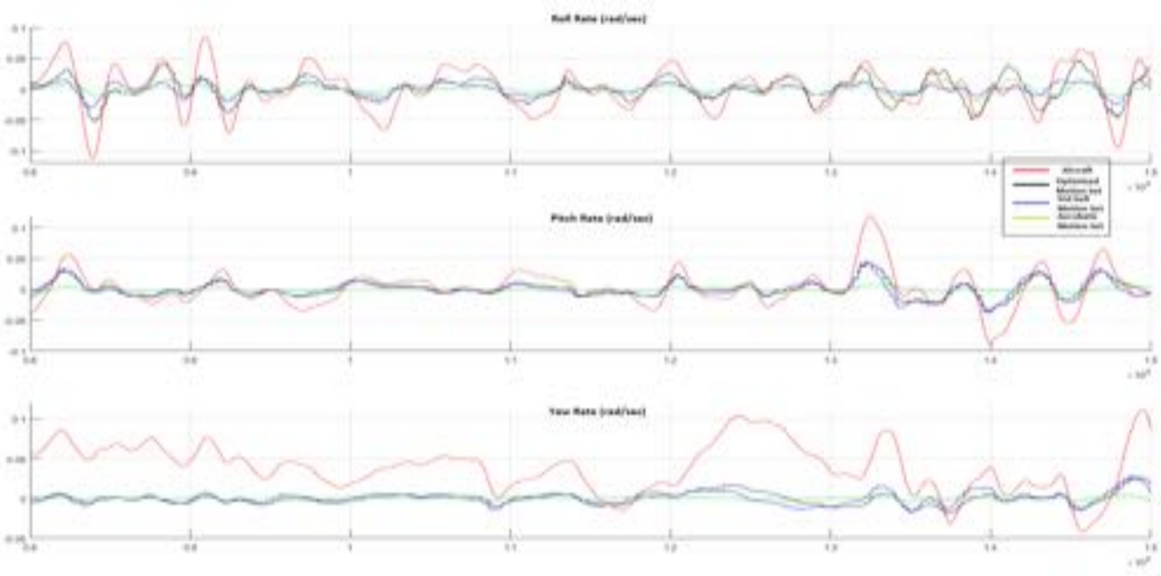

Fig. 7: Comparison of Angular Accelerations of Aircraft and Simulator Demands for Three Motion Tuning Sets

III. Future Work

Research is under process to develop robust fidelity matrices for rotorcraft flight simulation to optimise all the simulation elements and qualify overall fidelity of rotorcraft simulators. Further work is carried out to model optimal motion control high-pass and low-pass filters of 8th order based on minimization of a cost function using a solution of Algebraic Riccati Equation and Linear Quadratic Control.

IV. References

1. White, M.D., Perfect, P., Padfield, G.D. Gubbels, A.W., Berrymanm A.C.: Acceptance testing and commissioning of a flight simulator of rotorcraft simulation fidelity research. Proc. Inst. Mech, Eng. Part G J. Aerosp. Engi **227**(4) (2013).
2. Anon., "Strategic Research Agenda, Volume 1", Advisory Council for Aeronautics Research in Europe, October 2002.
3. Hess, R.A. and Malsbury, T., ""Closed Loop Assessment of Flight Simulator Fidelity", Journal of Guidance, Control and Dynamics. **14** (21) pp. 191-197, 1991.
4. Hess, R.A. and Suwakosit, W., "Assessment of Flight Simulator Fidelity in Multi-Axis Tasks Including Visual Cue Quality", Journal of Aircraft, Vol. 38, (4), pp. 607-614, 2001.
5. European Aviation Safety Agency "Authority and Organisation Requirements**",** Certification Specifications for Helicopter Flight Simulation Training Devices CS-FSTD (H)**,** 2008.
6. Hosman, R., Advani, S., "Design and Evaluation of Objective Motion Cueing Test and Criterion", The Aeronautical Journal, Vol.120, No.1227, Royal Aeronautical Society 2016.
7. Anon., "Aeronautical Design Standard Performance Specification Handling Qualities Requirements for Military Rotorcraft", ADS-33-PRF, United States Army Aviation and Missile Command, Redstone Arsenal, AL, 2000.

A High-Order Method for Rotorcraft Flow

Antonio Jimenez-Garcia* and George N. Barakos**

* PhD Student, *a.jimenez-garcia.1@research.gla.ac.uk* ** Professor, *George.Barakos@glasgow.ac.uk*
CFD Laboratory, School of Engineering, University of Glasgow, James Watt South Building, Glasgow G12 8QQ

1 INTRODUCTION

This work presents the development and implementation of an efficient, compact high-order finite-volume scheme in the HMB CFD solver. This formulation is based on the variable extrapolation MUSCL-scheme, where high-order spatial accuracy (up to 4th-order) is achieved using high-order correction terms through a successive differentiation. The scheme has also been modified to cope with physical and multiblock mesh interfaces, so stability, conservativeness, and high-order accuracy are guaranteed. A wide variety of results for the underlying method are presented, including two-and three-dimensional test cases. The convection of an isentropic vortex, and the aerodynamic interaction between a vortex and a NACA-0012 aerofoil (blade vortex interaction problem BVI) are first studied, demonstrating the high level of accuracy of the new formulation. Theoretical and numerical analyses of the truncation error are also included. The three-dimensional steady flows around the 7AD, S-76, and XV-15 blades are also computed. Results with the proposed scheme, showed better wake and higher resolution of the vortical structures compared with the standard MUSCL solution, even though a coarse mesh was employed. The method was also demonstrated to three-dimensional unsteady flows using overset and moving grid computations for the UH-60A rotor in forward flight.

2 HIGH-ORDER FORMULATION

This section describes the formulation of the high-order correction terms. This formulation was firstly proposed by Burg [1] for unstructured finite volume codes, where a third-order spatial accuracy was achieved for two-and three-dimensional problems. Yang *et al.*[2, 3] extended the scheme to fourth-order spacial accuracy. The scheme developed, closely resembles the MUSCL-schemes [4] (Monotonic Upstream-centered Scheme for Conservation Laws). This scheme is compact, and used here to discretised the convective part of the Navier–Stokes equations. It represents a one-parameter family of equations, where a third-order spatial accuracy can be achieved. For 1-dimensional problems and uniform spacing, the extrapolation to both sides of the face located at $i + 1/2$ for a MUSCL-scheme is given:

$$\begin{aligned}\mathbf{F}^L_{i+1/2} &= \mathbf{F}_i + \left[\frac{\kappa_1}{2}(\mathbf{F}_{i+1} - \mathbf{F}_i) + (1-\kappa_1)\vec{\nabla}\mathbf{F}_i \bullet \vec{\mathbf{r}}_{f_i}\right] \\ \mathbf{F}^R_{i+1/2} &= \mathbf{F}_{i+1} - \left[\frac{\kappa_1}{2}(\mathbf{F}_{i+1} - \mathbf{F}_i) + (1-\kappa_1)\vec{\nabla}\mathbf{F}_{i+1} \bullet \vec{\mathbf{r}}_{f_{i+1}}\right]\end{aligned} \tag{1}$$

which are at least second-order accurate for all values of k_1. By setting $k_1 = 0$, a 2nd-order upwind scheme is obtained. If $k_1 = 1/3$, the method is third-order accurate, which is referred in the literature to as ”third-order upwind biased” [5]. However, if k_1 is set to 1, a 2nd-order central difference scheme is obtained.

In the Eq. 1 the vectors $\vec{\mathbf{r}}_{f_i}$ and $\vec{\mathbf{r}}_{f_{i+1}}$ represent the distances between the cell-centre face $i + 1/2$ and cell-centre volume i, and the cell-centre volume $i + 1$ and cell-centre face $i + 1/2$, respectively. To reconstruct the gradients $\vec{\nabla}\mathbf{F}_i$ and $\vec{\nabla}\mathbf{F}_{i+1}$ at the cell-centre volumes i and $i + 1$, either Green-Gauss or Least-Squares approaches can be considered. It is clear that the present MUSCL-schemes is limited to third-order accurate.

Following Yang [2], the proposed 4th-order structured MUSCL scheme is written in a similar fashion, where the extrapolation to both sides of the face located at $i + 1/2$ is given as:

$$\begin{aligned}\mathbf{F}^L_{i+1/2} &= \overbrace{\mathbf{F}_i + \frac{\kappa_1}{2}(\mathbf{F}_{i+1} - \mathbf{F}_i) + (1-\kappa_1)\vec{\nabla}\mathbf{F}_i \bullet \vec{\mathbf{r}}_{f_i}}^{\text{Standard MUSCL for the left state}} \\ &\underbrace{+\frac{1}{2}\left[\frac{\kappa_2}{2}\left(\vec{\nabla}\mathbf{F}_{i+1} \bullet \vec{\mathbf{r}}_{f_i} - \vec{\nabla}\mathbf{F}_i \bullet \vec{\mathbf{r}}_{f_i}\right) + (1-\kappa_2)\vec{\nabla}\left(\vec{\nabla}\mathbf{F}_i \bullet \vec{\mathbf{r}}_{f_i}\right) \bullet \vec{\mathbf{r}}_{f_i}\right]}_{\text{High-order corrections for the left state}} \\ \mathbf{F}^R_{i+1/2} &= \overbrace{\mathbf{F}_{i+1} - \frac{\kappa_1}{2}(\mathbf{F}_{i+1} - \mathbf{F}_i) - (1-\kappa_1)\vec{\nabla}\mathbf{F}_{i+1} \bullet \vec{\mathbf{r}}_{f_{i+1}}}^{\text{Standard MUSCL for the right state}} \\ &\underbrace{+\frac{1}{2}\left[\frac{\kappa_2}{2}\left(\vec{\nabla}\mathbf{F}_{i+1} \bullet \vec{\mathbf{r}}_{f_{i+1}} - \vec{\nabla}\mathbf{F}_i \bullet \vec{\mathbf{r}}_{f_{i+1}}\right) + (1-\kappa_2)\vec{\nabla}\left(\vec{\nabla}\mathbf{F}_{i+1} \bullet \vec{\mathbf{r}}_{f_{i+1}}\right) \bullet \vec{\mathbf{r}}_{f_{i+1}}\right]}_{\text{High-order corrections for the right state}}\end{aligned} \tag{2}$$

As can be observed, this new variable extrapolation formulation represents a two-parameter family (k_1 and k_2), and is equivalent to the standard MUSCL-scheme under certain values of k_1 and k_2. As shown in the Eq. 2, the high-order correction terms have been developed using a Taylor series expansion about the centre of the face $i + 1/2$, which requires knowledge of its second derivate $\vec{\nabla}\big(\vec{\nabla}\mathbf{F}_i \bullet \vec{\mathbf{r}}_{f_i}\big)$. Once the first derivatives are computed, the second derivatives can be calculated by successive application of the Green-Gauss or Least Square Method to the first derivatives.

$$
\begin{aligned}
\mathbf{F}^L_{i+1/2} &= \mathbf{F}_i + \frac{\kappa_1}{2}(\mathbf{F}_{i+1} - \mathbf{F}_i) + (1-\kappa_1)\vec{\nabla}\mathbf{F}_i \bullet \vec{\mathbf{r}}_{f_i} \\
&+ \frac{1}{2}\left[\frac{\kappa_2 \Delta \mathrm{x}_{f_i}}{2}\left((\frac{\partial \mathbf{F}}{\partial \mathrm{x}})_{i+1} - (\frac{\partial \mathbf{F}}{\partial \mathrm{x}})_i\right) + (1-\kappa_2)\Delta \mathrm{x}_{f_i}\vec{\nabla}\left(\frac{\partial \mathbf{F}}{\partial \mathrm{x}}\right)_i \bullet \vec{\mathbf{r}}_{f_i}\right] \\
&+ \frac{1}{2}\left[\frac{\kappa_2 \Delta \mathrm{y}_{f_i}}{2}\left((\frac{\partial \mathbf{F}}{\partial \mathrm{y}})_{i+1} - (\frac{\partial \mathbf{F}}{\partial \mathrm{y}})_i\right) + (1-\kappa_2)\Delta \mathrm{y}_{f_i}\vec{\nabla}\left(\frac{\partial \mathbf{F}}{\partial \mathrm{y}}\right)_i \bullet \vec{\mathbf{r}}_{f_i}\right] \\
&+ \frac{1}{2}\left[\frac{\kappa_2 \Delta \mathrm{z}_{f_i}}{2}\left((\frac{\partial \mathbf{F}}{\partial \mathrm{z}})_{i+1} - (\frac{\partial \mathbf{F}}{\partial \mathrm{z}})_i\right) + (1-\kappa_2)\Delta \mathrm{z}_{f_i}\vec{\nabla}\left(\frac{\partial \mathbf{F}}{\partial \mathrm{z}}\right)_i \bullet \vec{\mathbf{r}}_{f_i}\right]
\end{aligned}
\tag{3}
$$

$$
\begin{aligned}
\mathbf{F}^R_{i+1/2} &= \mathbf{F}_{i+1} - \frac{\kappa_1}{2}(\mathbf{F}_{i+1} - \mathbf{F}_i) - (1-\kappa_1)\vec{\nabla}\mathbf{F}_{i+1} \bullet \vec{\mathbf{r}}_{f_{i+1}} \\
&+ \frac{1}{2}\left[\frac{\kappa_2 \Delta \mathrm{x}_{f_{i+1}}}{2}\left((\frac{\partial \mathbf{F}}{\partial \mathrm{x}})_{i+1} - (\frac{\partial \mathbf{F}}{\partial \mathrm{x}})_i\right) + (1-\kappa_2)\Delta \mathrm{x}_{f_{i+1}}\vec{\nabla}\left(\frac{\partial \mathbf{F}}{\partial \mathrm{x}}\right)_{i+1} \bullet \vec{\mathbf{r}}_{f_{i+1}}\right] \\
&+ \frac{1}{2}\left[\frac{\kappa_2 \Delta \mathrm{y}_{f_{i+1}}}{2}\left((\frac{\partial \mathbf{F}}{\partial \mathrm{y}})_{i+1} - (\frac{\partial \mathbf{F}}{\partial \mathrm{y}})_i\right) + (1-\kappa_2)\Delta \mathrm{y}_{f_{i+1}}\vec{\nabla}\left(\frac{\partial \mathbf{F}}{\partial \mathrm{y}}\right)_{i+1} \bullet \vec{\mathbf{r}}_{f_{i+1}}\right] \\
&+ \frac{1}{2}\left[\frac{\kappa_2 \Delta \mathrm{z}_{f_{i+1}}}{2}\left((\frac{\partial \mathbf{F}}{\partial \mathrm{z}})_{i+1} - (\frac{\partial \mathbf{F}}{\partial \mathrm{z}})_i\right) + (1-\kappa_2)\Delta \mathrm{z}_{f_{i+1}}\vec{\nabla}\left(\frac{\partial \mathbf{F}}{\partial \mathrm{z}}\right)_{i+1} \bullet \vec{\mathbf{r}}_{f_{i+1}}\right]
\end{aligned}
\tag{4}
$$

The present high-order formulation requires optimal values of k_1 and k_2 to assure higher-order of accuracy. In this regard, we derive the order of accuracy of the scheme in 1D, considering the approximation of the derivate at the nodes as:

$$
\begin{aligned}
&\int_{x-\frac{1}{2}}^{x+\frac{1}{2}} \frac{\partial \mathbf{F}}{\partial x} dx \approx \mathbf{F}^L_{i+\frac{1}{2}} - \mathbf{F}^L_{i-\frac{1}{2}} \\
&= \frac{1+\kappa_2}{32}\mathbf{F_{i+2}} + \frac{7+8\kappa_1-3\kappa_2}{32}\mathbf{F_{i+1}} + \frac{11-12\kappa_1+\kappa_2}{16}\mathbf{F_i} \\
&+ \frac{-19+12\kappa_1+\kappa_2}{16}\mathbf{F_{i-1}} + \frac{9-8\kappa_1-3\kappa_2}{32}\mathbf{F_{i-2}} + \frac{-1+\kappa_2}{32}\mathbf{F_{i-3}} \\
&= \mathbf{F}'_i \Delta x + \frac{1+6\kappa_1}{24}\mathbf{F}'''_i \Delta x^3 + \frac{1-2\kappa_1+\kappa_2}{16}\mathbf{F}^{(4)}_i \Delta x^4 + O(\Delta x^5)
\end{aligned}
\tag{5}
$$

One can observe that this formula is at least 2nd-order accurate for all values of κ_1 and κ_2, while if $\kappa_1 = -\frac{1}{6}$ and $\kappa_2 = -\frac{4}{3}$, the approximation of the derivate at the node is 4th-order accurate, with no mechanism of dissipation. Moreover, a low dissipation δ can be introduced to reduce spurious oscillation and at the same time maintain the high-order accuracy when κ_2 is set to $-\frac{4}{3}+\delta$.

3 XV-15 TILTROTOR BLADE

This section demonstrates the performance of the MUSCL-4 scheme with the chimera technique for a three-dimensional tiltrotor flow. The flow around the three-bladed XV-15 rotor [6] is solved in hover by casting the equations as a steady-state problem in a noninertial reference frame. The MUSCL-4 scheme is compared with the compact scheme MUSCL-2 in terms of integrated airloads (FoM, C_T, and C_Q), visualisation of the wake flow features, and wake structure (radial and vertical displacements of the vortex). All flow solutions were computed using RANS, coupled with Menter's k-ω SST turbulence model [7]. The flow equations were integrated with the implicit dual-time stepping method of HMB.

The three-bladed XV-15 rotor geometry comprises NACA 6-series five-digit aerofoil sections, and its main geometric characteristics [6] are summarised in Table 1. Regarding the test conditions, the blade-tip Mach number was set to 0.69, and five blade collective angles were considered ($\theta_{75} = 3°, 5°, 7°, 10°$, and $13°$), corresponding to low, medium, and high disc loadings. The Reynolds number, based on the reference blade chord of 14 inches and on the tip speed, was $4.95 \cdot 10^6$.

Table 1: Geometric properties of the full-scale XV-15 rotor [6].

Parameter	Value
Number of blades, N_b	3
Rotor radius, R	150 inches
Reference blade chord, c_{ref}	14 inches
Aspect ratio, R/c_{ref}	10.71
Rotor solidity, σ	0.089
Linear twist angle, Θ	-40.25°

The computational domain was composed by a cylindrical off-body mesh used as a background (Figure 1 (a)), and a body-fitted mesh for the blade with a C-H topology (Figure 1 (b)). Table 2 lists the grids used and the breakdown of cells per blade. Coarse and medium meshes have 6.2 and 9.6 million cells per blade (equivalent to 18.6 and 28.8 million cells for three blades), with the same grid resolution for the body-fitted mesh (3.6 million cells). The background mesh, however, was refined at the wake and near-body regions, increasing the grid size from 2.6 to 6 million cells. Solutions were obtained with the MUSCL-2 scheme using the coarse and medium grids, whilst the MUSCL-4 was only employed with the coarse grid.

Table 2: Mesh size in million cells for the XV-15 rotor mesh.

	Coarse Mesh	**Medium Mesh**
Background mesh size	2.6 million	6.0 million
Blade mesh size	3.6 million	3.6 million
Overall mesh size	6.2 million	9.6 million
Wall distance	$1.0 \cdot 10^{-5} c_{\text{ref}}$	$1.0 \cdot 10^{-5} c_{\text{ref}}$

Figure 2 shows the effect of the MUSCL-2 and MUSCL-4 schemes on the figure of merit and torque coefficient for the full-scale XV-15 rotor. Experimental data is also shown, carried out by Felker *et al.*[8] at OARF, and Light [9] and Betzina [6] at the NASA 80×120ft wind tunnel. Vertical lines labelled as empty (4,574 kg) and maximum gross (6,000 kg) weight, define the hovering range of the XV-15 helicopter rotor [10]. Momentum-based estimates of the figure of merit [11] are also included, where an induced power factor k_i of 1.1 and overall profile drag coefficient C_{DO} of 0.01 were used. Polynomial fit curves were computed using the obtained CFD results and shown with solid lines and squares (MUSCL-2 with a coarse grid), deltas (MUSCL-2 with a medium grid), and triangles (MUSCL-4 with a coarse grid). The CFD results obtained with the MUSCL-2 scheme present a good agreement with the test data of Betzina [6] for all blade collective angles. Moreover, the effect of the grid size has a mild effect on the overall performance at low thrust, with a small influence at high thrust. Regarding the results obtained with the MUSCL-4 scheme, a good agreement was obtained if compared with the MUSCL-2 scheme when using a medium grid, and the experimental data of Betzina.

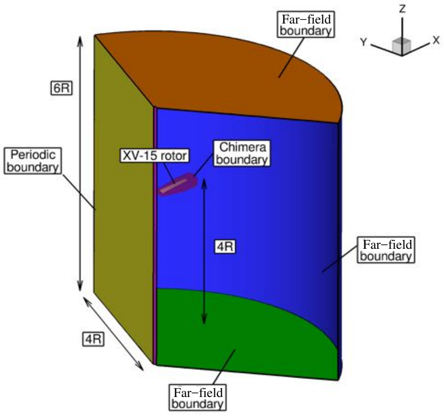

(a) Computational domain.

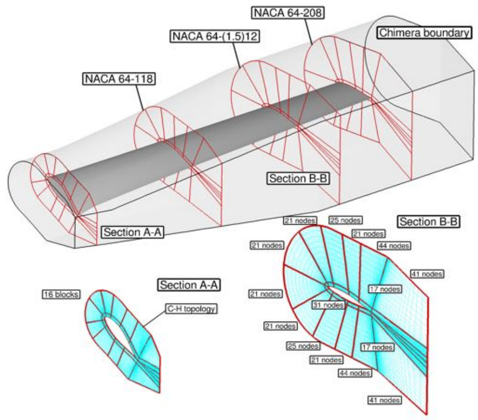

(b) XV-15 rotor mesh.

Figure 1: Computational domain and boundary conditions employed (above) and detailed view of the body-fitted XV-15 rotor mesh (below).

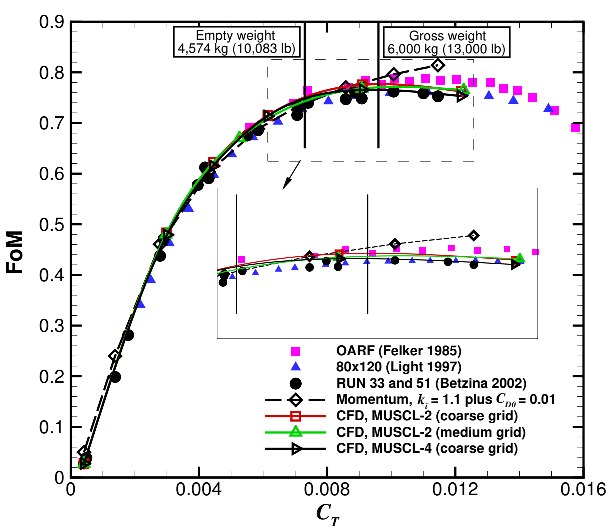

(a) FoM - C_T.

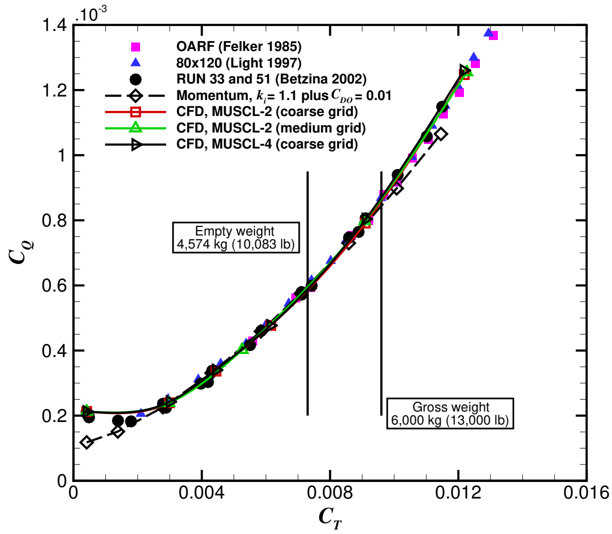

(b) C_Q - C_T.

Figure 2: Effect of the MUSCL-2 and MUSCL-4 schemes on the figure of merit (above) and torque coefficient (below) for the full-scale XV-15 rotor.

To assess the ability of the MUSCL-4 scheme in accurately predicting the loads when a coarse mesh is employed, a comparison between predicted and measured [12, 13] FoM at a collective pitch angle of 10° is reported in Table 3. Predictions with the MUSCL-2 scheme using coarse and medium grids indicate good correlation with the experiments (1.5 and 0.8 counts of FoM, respectively). Results obtained with the MUSCL-4 scheme on a coarse grid present a small discrepancy of 0.5 counts of FoM, which highlights the benefit of using higher-order numerical scheme in accurately predicting integrated airloads.

Table 3: Predicted and experimental [12, 13] figure of merit at collective pitch angle of 10°.

Case	FoM	Difference [%]
Experiment	0.760	-
MUSCL-2 coarse grid	0.775	1.97%
MUSCL-2 medium grid	0.768	1.05%
MUSCL-4 coarse grid	0.765	0.65%

Despite that the lower-order numerical scheme is sufficient to predict the loads over the blades [14], it did not preserve the near-blade and wake flow features. Those features play a key role in the prediction of the acoustic noise, BVI interactions, and in-ground effects. In hover, to ensure realistic predictions of the wake-induced effects and therefore induced-drag, the radial and vertical displacements of the vortex core should be resolved, at least for the first and second wake passages.

Figure 3 shows the wake flow-field for the full-scale XV-15 rotor using iso-surfaces of Q-criterion obtained with MUSCL-2 (a) and MUSCL-4 (b) with the same coarse grid of Table 2. It should be mentioned that, a collective pitch angle of 10° degrees was selected for such comparison. It is observed that the MUSCL-4 scheme preserves much better the helical vortex filaments that trail from each of the tip-blade, and the wake sheets trailed along the trailing edge of the blade if compared with the MUSCL-2 solution. Therefore, the lower dissipation of the MUSCL-4 scheme results in an improved preservation of rotor wake structures.

(a) Wake flow using MUSCL-2 scheme.

(b) Wake flow using MUSCL-4 scheme.

Figure 3: Wake flow-field for the full-scale XV-15 rotor using iso-surfaces of Q-criterion obtained with MUSCL-2 (above) and MUSCL-4 (below) schemes.

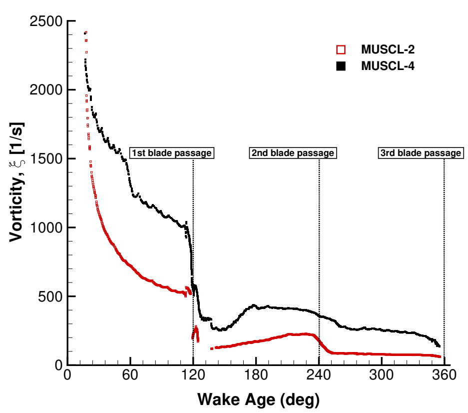

Figure 4: Vorticity of the vortex cores as function of the wake age in degrees obtained with the MUSCL-2 and MUSCL-4 schemes on the coarse grid.

Acknowledgements
The use of the cluster Chadwick of the University of Liverpool is gratefully acknowledged. Some results were obtained using the EPSRC funded ARCHIE-WeSt High Performance Computer (`www.archie-west.ac.uk`), EPSRC grant no. EP/K000586/1. Part of this work is funded under the HiperTilt Project of the UK Technology Strategy Board (TSB) and Leonardo Helicopters under Contract Nr. 101370.

REFERENCES

[1] Burg, C. O. E., "Higher Order Variable Extrapolation For Unstructured Finite Volume RANS Flow Solvers," *Proceedings of the Seventieth AIAA Computational Fluid Dynamics Conference*, AIAA, Toronto, Ontario, 2005, pp. 1–17.

[2] Yang, H. Q., Chen, Z. J., Przekwas, A., and Dudley, J., "A high-order CFD method using successive differentiation," *Journal of Computational Physics*, Vol. 281, No. 1, 2015, pp. 690–707, DOI: 10.1016/j.jcp.2014.10.046.

[3] Yang, H. Q. and Harris, R. E., "Vertex-centered, high-order schemes for turbulent flows," *Proceedings of the Fifty-Fourth Aerospace Sciences Meeting*, AIAA, San Diego, California, 2016, pp. 1–24.

[4] van Leer, B., "Towards the Ultimate Conservative Difference Scheme. V. A Second-Order Sequel to Godunov's Method," *Journal of Computational Physics*, Vol. 32, No. 1, 1979, pp. 101–136, DOI: 10.1016/0021-9991(79)90145-1.

[5] Anderson, W. K., Thomas, J. L., and van Leer, B., "Comparison of Finite Volume Flux Vector Splittings for the Euler Equations," *AIAA Journal*, Vol. 24, No. 9, 1986, pp. 1453–1460, DOI: 10.2514/3.9465.

[6] Betzina, M. D., "Rotor Performance of an Isolated Full-Scale XV-15 Tiltrotor in Helicopter Mode," *Proceedings of the American Helicopter Society Aerodynamics, Acoustics, and Test and Evaluation Technical Specialist Meeting*, AHS, San Francisco, CA, 2002, pp. 1–12.

[7] Menter, F. R., "Two-Equation Eddy-Viscosity Turbulence Models for Engineering Applications," *AIAA Journal*, Vol. 32, No. 8, 1994, pp. 1598–1605, DOI: 10.2514/3.12149.

[8] Felker, F. F., Betzina, M. D., and Signor, D. B., "Performance and Loads Data from a Hover Test of a Full-Scale XV-15 Rotor," NASA TM–86833, Sept. 1985.

[9] Light, J. S., "Results from an XV-15 Rotor Test in the National Full-Scale Aerodynamics Complex," *Proceedings of the 53rd American Helicopter Society Annual Forum*, AHS, Virginia Beach, Virginia, 1997.

[10] Maisel, M. D., Giulianetti, D. J., and Dugan, D. C., "The History of the XV-15 Tilt Rotor Research Aircraft: From Concept to Flight," NASA SP-2000-4517, 2000.

[11] Leishman, J. G., *Principles of Helicopter Aerodynamics*, Cambridge, 2000.

[12] Wadcock, A. J., Yamauchi, G. K., and Driver, D. M., "Skin Friction Measurements on a Hovering Full-Scale Tilt Rotor," *Journal American Helicopter Society*, Vol. 99, No. 4, 1999, pp. 312–319.

[13] Yoon, S., Pulliam, T. H., and Chaderjian, N. M., "Simulations of XV-15 Rotor Flows in Hover Using OVERFLOW," *Proceedings of the 50th AHS Aeromechanics Specialists*, AHS, San Francisco, CA, 2014, pp. 1–11.

[14] Ghosh, D., *Compact-Reconstruction Weighted Essentially Non-Oscillatory Schemes for Hyperbolic Conservation Laws*, Ph.D. thesis, University of Maryland, United States, Jan. 2013.

Analysis of Unsteady Aerodynamic Load of Tail Rotor under Main Rotor Aerodynamic Interaction with Vortex Method

1. Jianfeng Tan, Jianfengtan@njtech.edu.cn, School of Mechanical and Power Engineering, Nanjing Tech University, Nanjing 211816, R.P. China
2. George N. Barakos. George.Barakos@glasgow.ac.uk, CFD Laboratory, School of Engineering, University of Glasgow, Glasgow G12 8QQ, UK

The tip vortex of the main rotor can reach the tip path plane of the tail rotor in hover and side-slip conditions, which results in a marked variation of tail rotor unsteady aerodynamic loads. Analysis of the unsteady aerodynamic loads of a tail rotor, including the aerodynamic interactions between main rotor and tail rotor, is an essential part of tail rotor design.

In this work, an unsteady aerodynamic analysis of tail rotor is presented. The unsteady aerodynamic load of the tail rotor blade is modeled using an unsteady panel method, and the time-varying pressure induced by the main rotor tip vortex is also included to reflect the influence of the velocity impulse and time-varying geometry of the main rotor wake. Moreover, the interaction of the main rotor tip vortex with the tail rotor tip vortex is represented by vortex particle method.

As an example, the unsteady aerodynamic loads of the AH-1G main rotor blade are predicted in forward flight, and compared with experiments and CFD results to validate the effectiveness of the present approach. The influence of the main rotor wake on unsteady aerodynamic loads of tail rotor blade under hover, at crosswind and 60° starboard sideslip is analyzed base for the ROBIN rotor model. It is shown that the influence of the main rotor wake on the unsteady aerodynamic loads of the tail rotor blade is significant. The average tail rotor thrust coefficient is decreased, and its amplitude is increased under the interaction with the main rotor wake in hover. The “vortex ring” of tail rotor in portside crosswind is weakened by the interaction of main rotor tip vortex, and the average and amplitude of tail rotor thrust coefficient are significantly increased. The damage of tail rotor thrust is more prominent at 60° starboard sideslip, and thrust recovery is observed at low speed sideslip.

Figure 1 presents sectional airloads, including thrust coefficient and pitch moment coefficient, for the AH-1G main rotor blade in forward flight. It also presents comparisons between the current method and data from CFD results which show the potential of the proposed method.

Figure 2 shows the wake structure of the tail rotor during wake interaction with the main rotor. Comparing the wake of the isolated tail rotor with the wake structure of Main rotor/tail rotor Interaction (MTRI) is more complicated. The total thrust coefficient of the tail rotor with different wind directions is shown in Fig.3 together with the wake structure. The induced distribution of tail rotor in 60° right side with different forward flight is shown in Fig.4, while the time history and frequency of the tail rotor blade airloads in those situations are seen in Fig.5. It shows that the induced flow and unsteady aerodynamic loads of tail rotor is obviously influenced by main rotor.

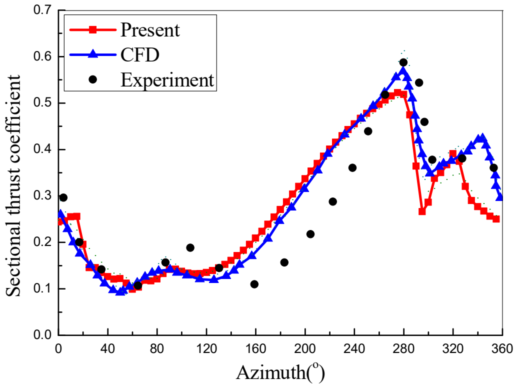

(a) Thrust coefficient

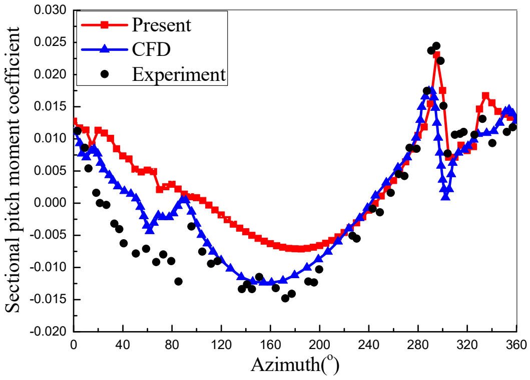

(b) Pitch moment coefficient

Fig.1 Time history of sectional airloads of the AH-1G main rotor blade.

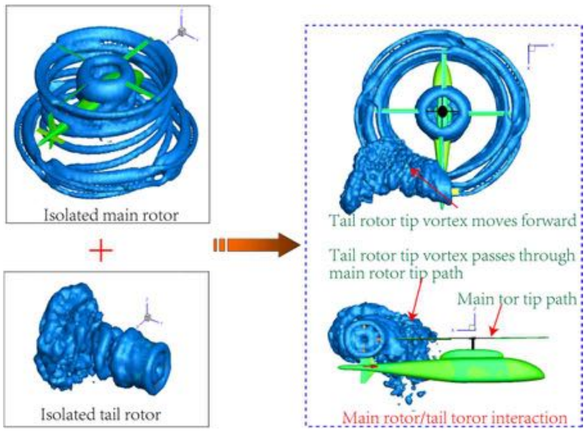

Fig.2 Wake structure of main rotor/tail rotor interaction in hover.

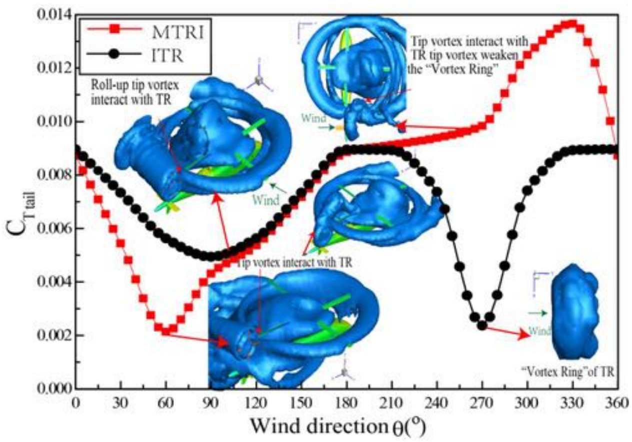

Fig.3 Total thrust coefficient of tail rotor at different wind directions.

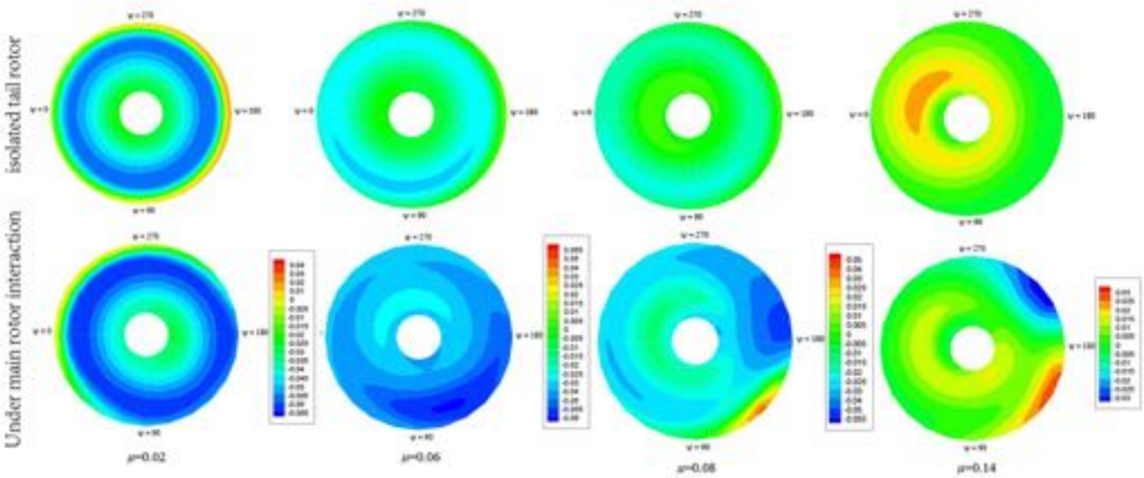

Fig.4 Induced velocity of tail rotor at 60° right side at different forward flight speeds.

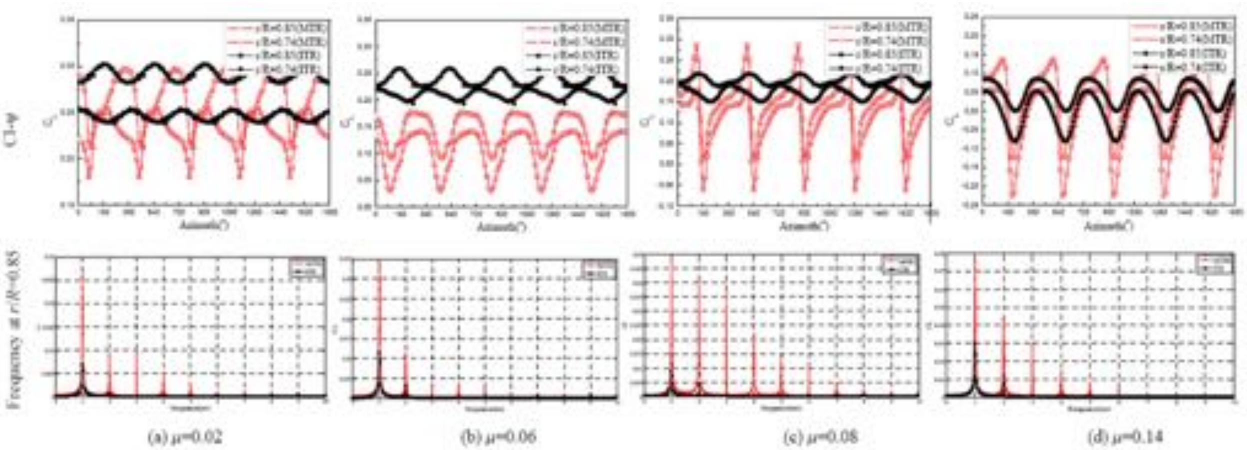

Fig.5 Time history and frequency of tail rotor blade airloads at 60° right side at forward flight speeds.

UK Vertical Lift Network Annual Technical Workshop
May 2017, Cheshire, UK

Aeromechanics of Tilt-Rotor Aircraft

Wesley Appleton and Antonio Filippone
The University of Manchester

The conversion corridor is the transition between the helicopter and aeroplane modes of operation for tilt-rotor aircraft. This research project focuses on the development of an aeromechanics model that captures the variation of thrust, torque and power requirements throughout the corridor. Accurate modelling is critical to ensure aircraft safety and bridge the flight envelopes of rotorcraft and propeller driven, fixed wing aeroplanes. The rotation of the engine nacelle distorts the flowfield through the proprotor creating a large degree of flow unsteadiness. Consequently, the proprotor loading is also unsteady and this has a significant effect on the aeromechanic performance during the conversion. These unsteady effects are transient and subside in the aeroplane mode operation, however, they exist continually in helicopter mode due to the presence of the wing in the proprotor wake.

The literature on aeromechanics during the conversion corridor is scarce. Very few models exist that describe the induced velocity variation [1, 2] and the aeromechanics during the conversion phase, providing strong justification for the current research project. Several quasi-steady, fixed nacelle simulations have been completed using CFD or performance analysis codes [3, 4, 5, 6] and the results generally show good correlation to experimental investigations. More recently, unsteady studies of the conversion corridor have been undertaken that have showed the flowfield unsteadiness to have a significant influence on the proprotor performance, particularly in the initial transition stage.

The current model utilises the traditional blade element theory combined with Glauerts momentum theory [7] for rotorcraft in forward flight. The momentum theory is constructed in an annular formation that allows a radial induced velocity distribution to be evaluated by iteratively solving Equations 1 and 2. Presently, the model assumes a quasi-steady flowfield and has been used to calculate the axial and tangential induced velocity distributions for any nacelle angle and freestream velocity, based on the configuration data in [8]. The initial results indicated a straight, level conversion corridor produces a portion of negative blade loading towards the tip region due to large negative angle of attacks, a result also noted by [9]. To overcome this adverse effect, additional blade collective is required which consequently increases the thrust produced. Hence, an alternative flight regime, such as an oblique climb with a negative aircraft pitch attitude, may be more practical during the conversion corridor.

$$v_i V_{disc} - \frac{\sigma}{8\pi} \int_0^{2\pi} W^2 (C_L \cos\phi - C_D \sin\phi) \kappa \, d\psi = 0 \tag{1}$$

$$v_\psi - \frac{\sigma}{8\pi V_{disc}} \int_0^{2\pi} W^2 (C_L \sin\phi + C_D \cos\phi) \kappa \, d\psi = 0 \tag{2}$$

An analysis of the reduced frequency over the entire conversion corridor showed highly unsteady flow existed at all radial and azimuthal blade stations. Therefore, the unsteady influence of the near-wake must be considered to develop an accurate engineering model. Furthermore, a significant quantity of aerodynamic interaction exists during the initial transition into the corridor. This is due to the wing being submerged in the wake of the proprotor and this creates both wing download and a downwash velocity. As the nacelle angle increases, the collective input has less impact on the proprotor lift production and therefore the conversion speed should be achieved as quickly as possible. Within the low speed flight region, most of the unsteady, interactional aerodynamics exist and hence, sufficient modelling is required in this critical region of conversion.

References

[1] P. B. Harendra, M. J. Joglekar, T. M. Gaffey, and R. L. Marr, "A Mathematical Model For Real Time Flight Simulation of the Bell Model 301 Tilt Rotor Research Aircraft," tech. rep., 1973.

[2] X. Wang and L. Cai, "Mathematical modeling and control of a tilt-rotor aircraft," *Aerospace Science and Technology*, vol. 47, pp. 473–492, 2015.

[3] Y. Zhang, L. Ye, and S. Yang, "Numerical study on flow fields and aerodynamics of tilt rotor aircraft in conversion mode based on embedded grid and actuator model," *Chinese Journal of Aeronautics*, vol. 28, no. 1, pp. 93–102, 2015.

[4] F. Nannoni, G. Giancamilli, M. Cical, and C. Costa, "ERICA: The European Advanced Tiltrotor," Tech. Rep. September, European Rotorcraft Forum, 2001.

[5] J. Decours and T. Lefebvre, "Navier Stokes computations Applied to tilt-rotors," tech. rep., European Rotorcraft Forum, 2007.

[6] G. Barakos and J. Garcia, "CFD Simulations on the ERICA tiltrotor using HMB2," *American Institute of Aeronautics and Astronautics*, no. 54th, 2016.

[7] H. Glauert, "On the Horizontal Flight of a Helicopter," tech. rep., 1928.

[8] F. Felker, M. Betzina, and D. Signor, "Performance and Loads Data from a Hover Test of a Full-Scale XV-15 Rotor," *NASA Technical Memorandum 86833*, 1985.

[9] W. Johnson, "Calculation of the Aerodynamic Behavior of the Tilt Rotor Aeroacoustic Model (TRAM) in the DNW," in *American Helicopter Society 57th Annual Forum*, (Washington), 2001.

Numerical and Experimental Comparison of a Carrier Air-wake for use in Fixed-Wing and Rotary-Wing Flight Simulation

Neale A. Watson1*, Mark D. White and Ieuan Owen

Flight Science & Technology, School of Engineering, University of Liverpool

This work investigates the aerodynamics of the Queen Elizabeth Class (QEC) aircraft carrier. The unsteady flow over the ship has been modelled using Computational Fluid Dynamics (CFD). This large and complex flow field solution will be incorporated into the Heliflight-R simulator at the University of Liverpool to identify areas of increased disturbance requiring high pilot workload prior to First of Class Flight Trials. Deployed aircraft to QEC will include Apache, Wildcat, Merlin, Chinook and the Advanced Short Take-Off and Vertical Landing (ASTOVL) variant of the Lockheed Martin F-35 Lightning II.

The Delayed Detached Eddy Simulation (DDES) SST k-ω based turbulence model in ANSYS Fluent was used to compute the very large and complex flow field. A large mesh in the order of 120 million cells is needed to accurately resolve the flow. High Performance computing (HPC) was required to solve the simulation using CHADWICK at the University of Liverpool.

In order to compare the CFD solution with experimental data a 3D printed 1:202 scale model of the aircraft carrier was placed in the University of Liverpool's water channel. Mean and turbulent velocities were measured through the use of Acoustic Doppler Velocimetry (ADV). ADV uses the acoustic Doppler technique to measure velocity components in three different directions simultaneously. The water channel is seeded with buoyancy neutral particles to reflect the acoustic signals to the receivers.

ADV measurements were taken at interval heights behind the islands of the ship and the mean and turbulent velocities compared with results from the CFD solution. Figure 2 shows a comparison of the x velocity profile behind the forward and aft islands of the QEC.

(a) (b)

Figure 1 (a) Computer-generated image of flight deck operations on the aircraft carrier HMS Queen Elizabeth (b) 3D printed scale model of QEC in water channel with ADV probe between the two islands

* School of Engineering, Brownlow Hill, Liverpool, L69 3GH Email: nawatson@liv.ac.uk

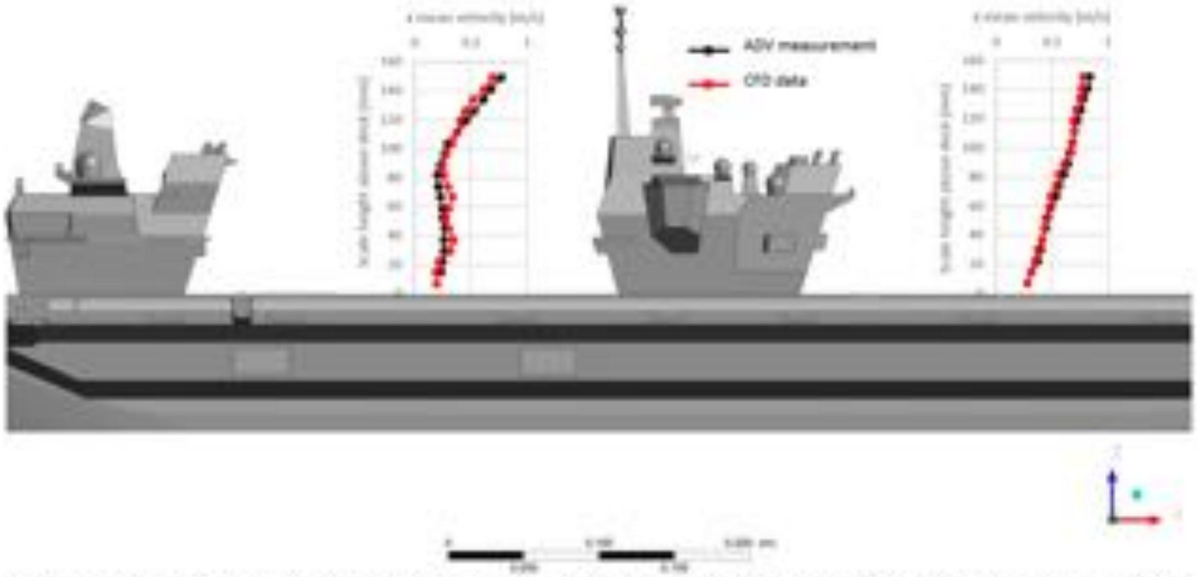

Figure 2 ADV measurement and CFD solution mean x velocity profile comparison behind the forward and aft island of the QEC.

References

[1] M F Kelly, M D White, I Owen and S J Hodge, *"The Queen Elizabeth Class Aircraft Carriers: Airwake Modelling and Validation for ASTOVL Flight Simulation"* American Society of Naval Engineers Launch & Recovery Symposium 2016

[2] J S Forrest, C H Kaaria, I Owen, *"Evaluating ship superstructure aerodynamics for maritime helicopter operations through CFD and flight simulation"* The Aeronautical Journal, available on CJO 2016 doi:10.1017/aer.2016.76 (July 2016).

[3] P R Spalart, S Deck, M L Shur, K D Squires, M Kh Strelets, A Travin, *"A New Version of Detached-Eddy Simulation, Resistant to Ambiguous Grid Densities."* Theoretical and Computational Fluid Dynamics, Vol. 20, Issue 3, pp. 181. July 2006.

[4] Gov.uk. 2015. *Crowsnest - the 'eyes and ears' of the fleet*. [ONLINE] Available at: https://modmedia.blog.gov.uk/2015/05/22/crowsnest-the-eyes-and-ears-of-the-fleet/. [Accessed 5 April 2017].

Vibration Control Software Development and System Integration for an Active Trailing Edge System to Reduce Helicopter Noise and Vibration

T. S. Magowan[1], D. E. Clark[1], P. A. Court[1]

1. Leonardo Helicopters.
Yeovil BA20 2YB, UK
http://www.leonardocompany.com/

Helicopter vibration is generated as a result of flying the main rotor edgewise so that there is periodic excitation of the blades at harmonics of the rotor rotational frequency. These rotating frame forces induce vibration in the airframe only at harmonics of the blade passing frequency e.g. 5 per rev for a 5 bladed rotor. Benefits in reducing airframe vibration include the extension of component fatigue lives and increased passenger comfort. Active vibration control offers an alternative to more conventional passive vibration absorbers which are heavy and can only be tuned to the main blade passing frequency of the helicopter. An active trailing edge system alternatively has the ability to control multiple forcing frequencies on the airframe.

The active trailing edge (ATE) system was developed by Leonardo Helicopters in the Rotorcraft Technology Validation Programme (RTVP) which aims to develop, test and assess the benefits of ATE technology on a demonstrator aircraft. It employs the use of trailing edge flaps mounted to the inboard and outboard sections of the blades (Figure 1). Each blade contains a set of 2 inboard flaps and 1 outboard flap. These flaps are actuated using electro-mechanical actuators mounted inside the blades. The benefits of an active trailing edge system over other active systems is that it reduces vibration aerodynamically at its source, making it a lighter and more energy efficient system than those currently employed.

Cabin vibration is controlled using a Vibration Management Computer (VMC) which measures airframe vibration from a set number of accelerometers mounted around the cabin. A Filtered X LMS algorithm is then used for closed loop control, generating blade position demands, which are transmitted to an actuator power and control unit that provides the inner loop control of the actuator positions.

The VMC software has been developed using hardware in the loop (HIL) principles where, on the test rig, the VMC transmits blade demands to an XPC target machine which runs a plant model to simulate the cabin vibration generated by the rotor. Cabin vibration is measured in the fixed frame, whereas the actuator forces are generated in the rotating frame. The plant model demodulates the blade demands from the rotating frame to drive a state space model simulating the response of each cabin accelerometer in the fixed frame. These accelerations are transmitted back to the VMC closing the loop. Both the VMC and XPC plant model run in real time allowing for the testing of the real time performance of the software.

As well as simulating cabin vibration, the XPC plant model has been developed as a tool to integrate the VMC with the other interfaced equipment that make up the active vibration control system. This is achieved through simulations of the actuator power and control unit, positon and temperature sensors, air data and rotor synchronisation hardware. The test rig also has the functionality to substitute the XPC machine with the real interfaced equipment to test the VMC's performance with the real hardware, and to validate simulations in the XPC plant model.

The development process has yielded an algorithm which successfully controls vibration in the HIL configuration on the test rig. The active rotor blades have been manufactured and tested on the aircraft. The next steps for the programme are to certify the VMC software ready for integration on the aircraft and flight testing.

Acknowledgements
The financial support from Innovate UK for the Rotor Technology Validation Programme is gratefully acknowledged

Figure 1 - Active Trailing Edge blade showing the inboard and outboard flaps painted red

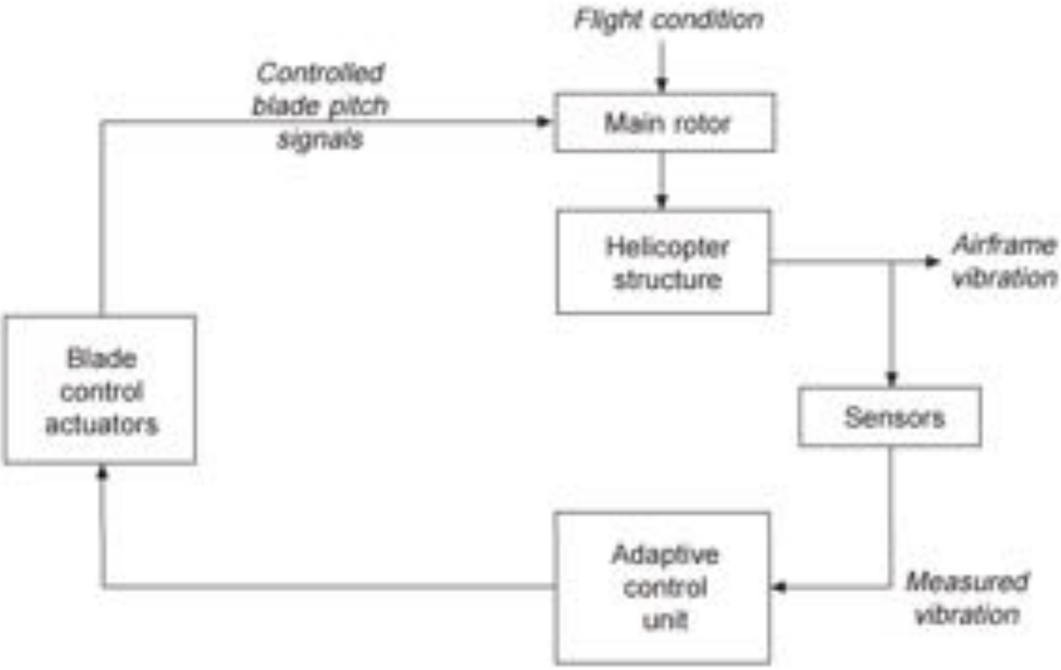

Figure 2 - Active vibration control system overview

Active Blade Twist and Advanced Rotor Tip Design

Mark A. Woodgate* and George N. Barakos**

* Research Associate, *Mark.Woodgate@glasgow.ac.uk*
** Professor, *George.Barakos@glasgow.ac.uk*

CFD Laboratory, School of Engineering, James Watt South Building,
University of Glasgow, Glasgow, G12 8QQ, U.K.

1 Abstract

Technologies that expand the helicopter flight envelope and deliver better performance are highly sought after by the helicopter industry. Due to their primary importance, the main rotor blades are seen as one of the helicopter components where large benefits can be obtained using modern computer simulation and optimization. Efforts to deliver better passive and active blades designs are currently underway all around the world with several collaborative efforts also reported. Looking at blade shape optimization, the work of Johnson and Barakos [1], used high fidelity computational fluid dynamics in conjunction with artificial neural networks as meta-models of the blade performance, and genetic algorithms to optimise the planform for the blade for maximum performance in both hover and forward flight. This approach has also been used by manufacturers to deliver blades of advanced planforms [2]. Active blade solutions are also under investigation, and are expected to deliver efficient designs since the blades can adapt to their operating environment and flight conditions. However an active solution is expected to be more expensive, add extra weight to the blades, require additional power for the active control, and probably increase maintenance costs.

The Rotor Embedded Actuator Control Technology (REACT) programme, funded by Innovate UK and AgustaWestland (now Leonardo MW) , explored technologies and capabilities to provide the groundwork towards developing future generation flight trialed active rotor technologies. Outside the UK, the Blue Pulse™ [2] project objectives were to reduce noise levels due to BVI, to increase aerodynamic performance of the rotor by either alleviating the dynamic stall of the blade or decreasing the consumed power in fast cruise flight, and reduce vibrations within the helicopter airframe, increasing passenger comfort and reducing component fatigue. The system used three trailing edge flaps on each rotor blade which changed the vortex convection between blades increasing the distance between the blade and the vortex.

The STAR [3] (Smart Twisting Active Rotor) is another research effort aiming to actively change the blade twist around the azimuth. This can be achieved by either a direct aerodynamic effect on the blade twist or by inducing a modified aeroelastic response by changing the blade stiffness.

The tips play a very important role in the aerodynamic performance of the rotor as this is where the highest Mach number, and pressure gradients are seen, In addition, the tips generate strong tip vortices that dominate the rotor wake system. Advanced designs have some combination of sweep, taper and anhedral and many even involve large changes in planform. One blade with a unique planform is the British Experimental Rotor Programme (BERP) blade. The program started in the late 1970's as a collaboration between Westland Helicopters and the Royal Aircraft Establishment with the goal of increasing the helicopters maximum take off weight and maximum speed using new a design and materials. The BERP tip was designed for high-speed forward flight without compromising hover performance [4]. It used thinner aerofoil sections, reduced blade stall, and the planform was optimized using a notch and a swept tip to reduce high Mach number effects while maintaining the position of the aerodynamic center.

The Blue Edge™ rotor was designed at ONERA and DLR during the ERATO program [5]. The idea behind the double-swept shape was to reduce the noise generated by blade-vortex interactions (BVI), which occur when a blade encounters a vortex created at the tip of the blade. An inboard forward sweep is followed by an outboard backward sweep with the span-wise chord, twist and thickness distributions were optimized to reduce the intensity of the emitted vortices.

This project aims to combine passive blade optimization of an advanced blade planform with active elements, and in particular with active twist. To achieve this, a CFD tool coupled with aeroelastic and aero-servo-elastic models is put forward. Results from CFD simulations are shown in Figures 1 and 2 where BERP-like and swept-back tips are compared, and the flow near the tip of a BERP-like blade is visualised.

Acknowledgements
This project is supported by the Defense Science and Technology Laboratory (DSTL) of the U.K.

References

[1] Johnson, C. and Barakos, G., "Optimizing Rotor Blades with Approximate British Experimental Rotor Programme Tips," *Journal of Aircraft*, Vol. 51, No. 2, 2014, pp. 447–463.

[2] Konstanzer, P., Enenkl, B., Aubourg, P., and Cranga, P., "Recent advances in Eurocopter's passive and active vibration control," *Proceedings of the 64th Annual Forum of the American Helicopter Society*, 2008.

[3] Bauknecht, A., Ewers, B., Schneider, O., and Raffel, M., "Aerodynamic Results from the Star Hover Test: An Examination of Active Twist Actuation," 41st European Rotorcraft Forum, Munich, Germany, September, 2015.

[4] Harrison, R., Stacey, S., and Hansford, B., "BERP IV-the design, development and testing of an advanced rotor blade," *Proceedings of the 64th Annual Forum of the American Helicopter Society*, 2008.

[5] Rauch, P., Gervais, M., Cranga, P., Baud, A., Hirsch, J., Walter, A., and Beaumier, P., "Blue edge: the design, development and testing of a new blade concept," *Proceedings of the 67th Annual Forum of the American Helicopter Society*, 2011, pp. 542–555.

(a) Generic BERP shape

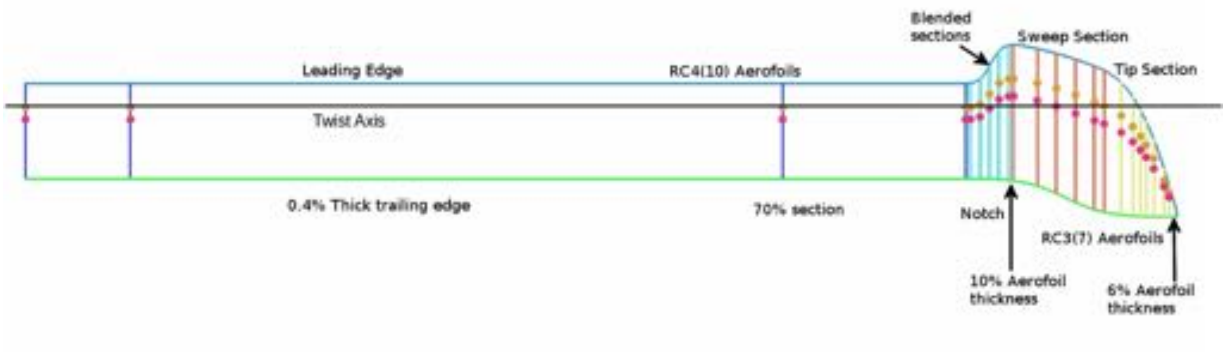

(b) Langley BERP shape

Figure 1: A BERP-like rotor in comparison to a swept tip design.

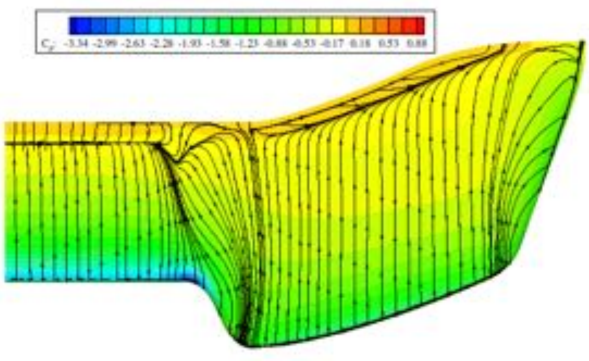

(a) 15.0^o Flap up

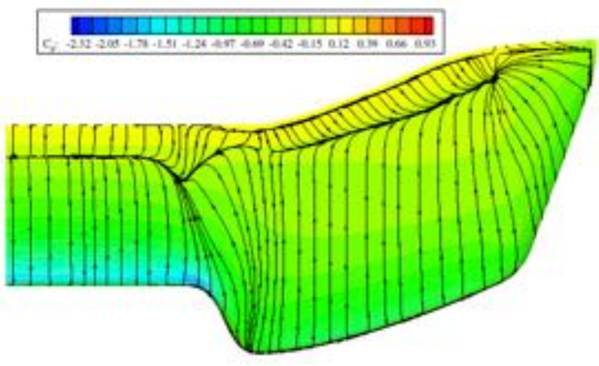

(b) 10.0^o Flap down

Figure 2: Velocity distribution and Pressure coefficient thought the tip region of a generic BERP rotor blade at Mach number 0.15

UK Vertical Lift Network Annual Technical Workshop
22-23 May 2017

Analytical Modeling of a Composite Fish Bone Active Camber Morphing Aerofoil for Application to Active Helicopter Rotors

A.E. Rivero
and
P.M. Weaver, J.E. Cooper and B.K.S. Woods

Abstract

Variable camber aerofoils have the capability to adapt the aerodynamic profile of a wing to different flight scenarios. This is potentially very useful within rotorcraft applications as it allows for the blade to adapt to both quasi-static changes in the required thrust level of the rotor and to time varying operating conditions around the azimuth. The Fish Bone Active Camber (FishBAC) concept is a biologically inspired morphing trailing edge device that is able to produce large, smooth and continuous changes in camber distribution. It consists of a central spine that acts as the main load bearing member of the structure, a series of spanwise stringers that provide both skin support and spanwise stiffness and an elastomer-based skin. The FishBAC is actuated by using two rotational servos, at both spanwise ends of the wing, that drive a pair of antagonist tendons that are connected to the trailing edge of the aerofoil (Figure 1. Structural configuration of the Fish Bone Active Camber (FishBAC) morphing trailing edge device.

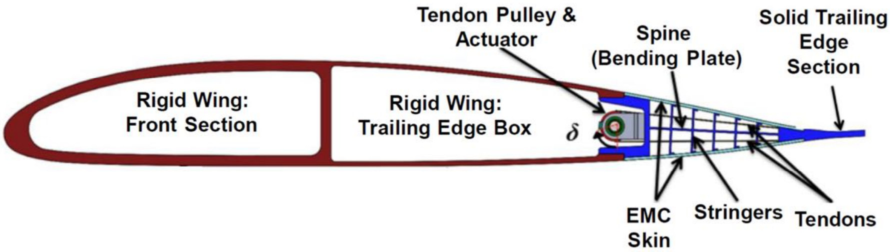

Figure 1. Structural configuration of the Fish Bone Active Camber (FishBAC) morphing trailing edge device

Preliminary structural design and analysis of the FishBAC was performed using a 1-dimensional model based on Euler-Bernoulli Beam theory. Although its computational efficiency and ability to capture chordwise stiffness variations, the model lacks the ability to capture variations in spanwise deformation due to either 3D aerodynamic loads or due to the twist induced by asymmetric actuation inputs. Furthermore, a 1-dimesional structural model lacks the ability to fully capture the mechanics of FishBAC spines manufactured with composite layups.

To address these shortcomings, a two-dimensional structural model based on Kirchhoff-Love plate theory has been developed. The model captures the complex geometry and large discontinuities in stiffness (due to the stringers, for example) of the FishBAC by discretizing the structure into a series of individual plates of locally uniform stiffness. The plate's differential equation is solved in each individual plate by performing an energy balance using Rayleigh-Ritz Method (i.e. Principle of Minimum Potential Energy) and then the individual plates are joined together using a series of penalty springs according to Courant's Penalty Method.

Furthermore, the developed model has the ability to analyse fully orthotropic plates, using Classical Laminate Theory (CLT), and can be used as a design and optimisation tool, as it is able to rapidly modify the geometric and material parameters of the FishBAC (e.g. thickness and spacing of stringers, skin and stringers' material, spine's stacking sequence, etc.).

To validate this analytical approach, a Finite Element Model of the FishBAC was also developed using ABAQUS/CAE version 6.14-1. Analysis of a wide range of spine composite layups and load cases shows that the analytical model can predict deflections due to uniform transverse pressure with less than 3% error and deformations due to both uniform (i.e. both actuators generating equal amount of torque) and non-uniform actuation inputs with less than 10% error. It is important to point out that the analytical model solves the FishBAC's displacement field using less than 1% of the degrees of freedom (DOF) required in the FEM model.

Figure 2 shows an example of the convergence studies performed, where a spine with stacking sequence *[45/45/45]$_s$* was subjected to uniform pressure distribution. Figure 3 presents a comparison of displacement fields of a *[90/90/90]$_s$* FishBAC's spine under non-uniform actuation loads.

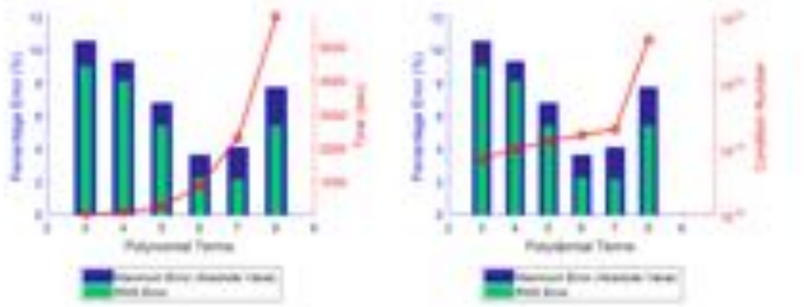

Figure 2. Comparison between analytical and FEM results for a spine's stacking sequence of [45/45/45]$_s$

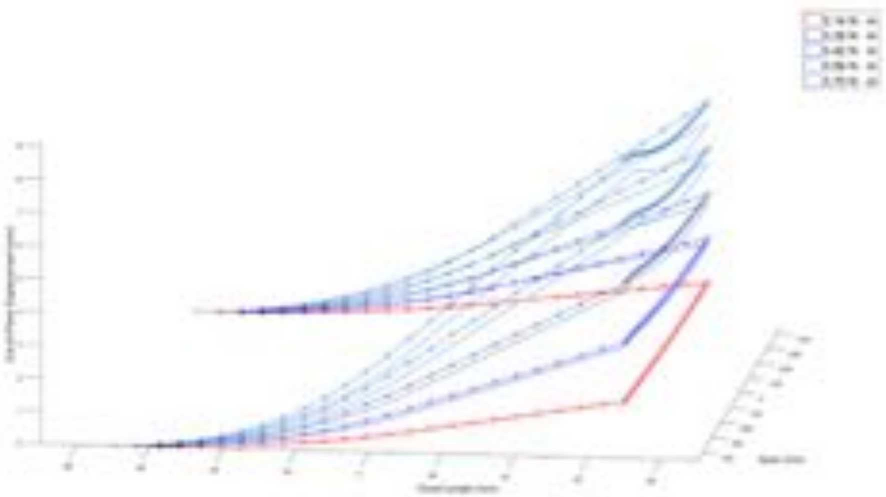

Figure 3. FEM (o) vs. Analytical (solid) displacement fields of a [90/90/90]$_s$ spine under non-uniform actuation loads. The outermost actuator's torque is varied between 0.14 and 0.7 Nm, while the innermost actuator exerts no torque.

This analytical model will serve as the basis for development of a coupled Fluid-Structure Interaction (FSI) analysis to study the aeroelasticity and dynamic behavious of the FishBAC. Future work will also validate this model against wind tunnel experiments.

Detection of a defective bearing on a civil aircraft engine using vibration analysis

J. L. du Bois[1] , L. Barbini[1]

Condition monitoring consists of determining the state of the components of a machine while it is in operation. Compared to scheduled maintenance and inspection, condition monitoring has the potential to contribute significant savings. However the complexity of the signals to be analysed typically requires the use of dedicated digital signal processing units overseen by skilled operators, and effective savings can be achieved only through the automation of the condition monitoring process. In addition it is preferable to have a condition monitoring unit which can produce warnings at any time throughout the operation of the machine, without operator oversight.

The literature offers a wide range of digital signal processing algorithms for condition monitoring [1]. In real world applications, as for instance condition monitoring of a helicopter gearbox [2] or of a civil aircraft engine [3], the complexity of such algorithms is directly related to their ability to detect damage, but with increasing complexity the algorithms become increasingly difficult to automate. In contemporary commercial condition monitoring systems the automation is achieved using relatively simple algorithms, to the detriment of detection capabilities. This results in missed detection of faults and in catastrophic failures, as in the 2009 accident of the Super Puma G-REDL helicopter [4], where the condition monitoring system was not able to warn of a defective planet gear bearing [5].

Therefore there is the need for an easy-to-automate algorithm which has a performance comparable to that of more complex ones. This presentation demonstrates the newly-developed Amplitude-cyclic frequency Decomposition (AD) and shows that it is easy to automate and offers good performance. AD is applied to detect a defective bearing in a civil aircraft engine operating at variable speed. The data used in in this work was provided by Safran; it consists of a vibration signal acquired at 50 kHz by an accelerometer and a tachometer signal for speed recovery.

When a bearing is defective it does not operate smoothly but generates a series of impacts. Each impact produces vibrations which propagate from the bearing to the vibration transducer. Diagnosis of a defective bearing consists of the detection of such vibrations from the spectral analysis of the data collected by the transducers. However a transducer gathers vibrations from all the components of the machinery, for example gears in the case of bearings supporting a shaft in a gearbox. Therefore pre-processing techniques are applied to the raw vibration signal to enhance the signal component from the bearing. The classical approach consists of band pass filtering around the resonant frequency excited by the impacts from the defective bearing. However the optimal band is unknown *a priori* and depends on the defect itself, so that a filter bank is blindly applied. This approach is computationally expensive and it is only recently that an algorithm of reasonable computational speed has been introduced [6]. The approach presented here on the other hand exploits the fact that vibrations from a defective bearing have small amplitude compared to that of vibrations from other components. Therefore it consists of a thresholding in the amplitudes of the spectral components of a signal versus the band pass filtering of the classical approach. The results achieved by AD on the civil aircraft engine are comparable to those of the state of the art technique [6], but the approach proposed here offers two advantages. Firstly a lower number of thresholds in the amplitudes of the spectral components versus the number of band pass filters is needed to achieve the same results. Secondly AD relies only on the Fast Fourier Transform algorithm, which is commonly used in many digital signal processing units.

[1] University of Bath, dept. Mechanical Engineering, Claverton Down, Bath, BA2 7AY, UK

The results are shown alongside the experimental setup in Figure 1. On the first row it shows the schematics of the civil engine aircraft, on the second row the proposed AD method and the Spectral Coherence (SC)[6]. On the third row the integral of the AD in a range of spectral amplitudes and the enhanced envelope spectrum obtained from the spectral coherence. BPOO is the Band Pass Outer Order corresponding to the occurrence frequency of the impacts from the defect on the outer race of the bearing, divided by the mean rotational frequency of the shaft where the bearing is mounted. CO corresponds to the Cage Orders.

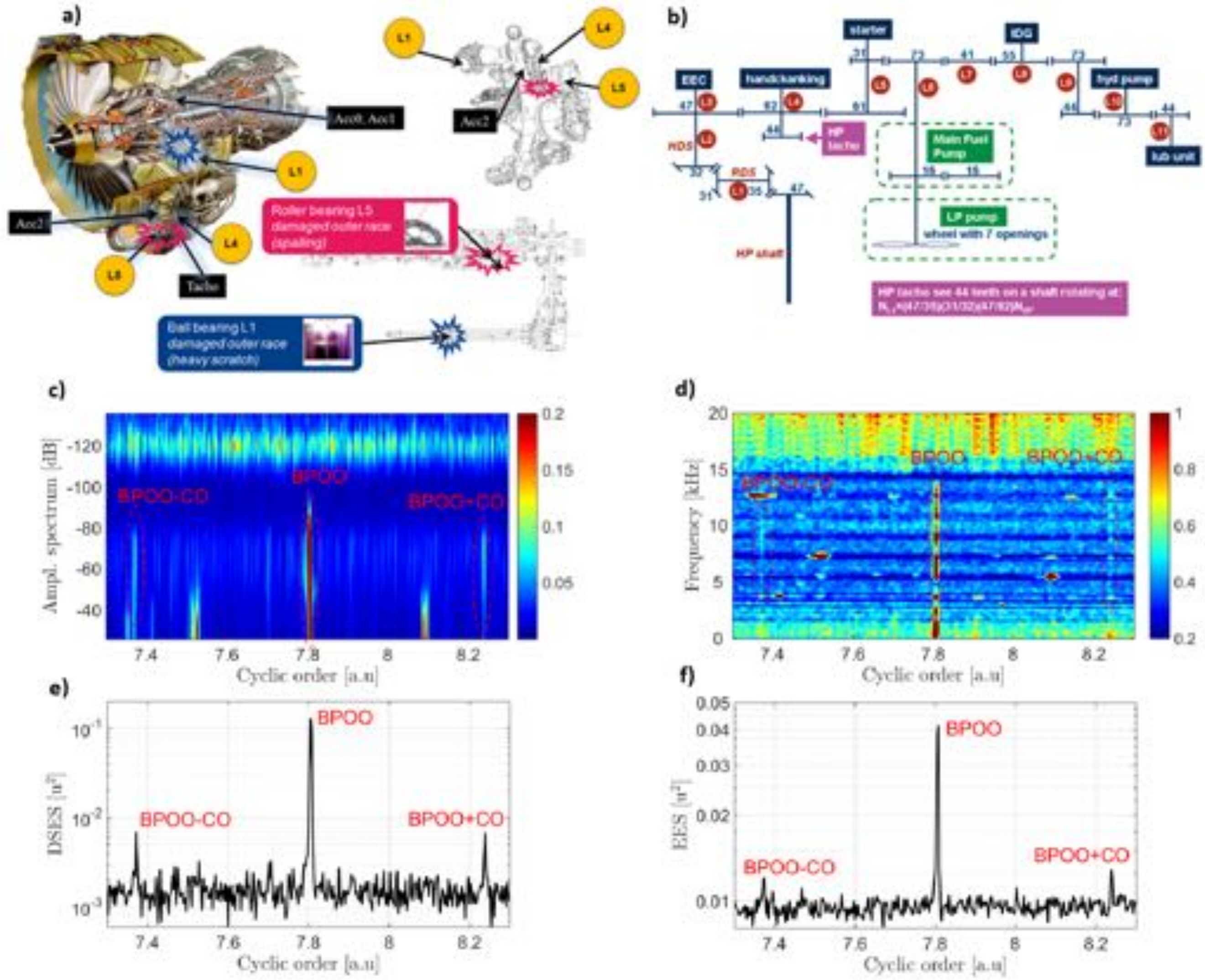

Figure 1. (a) General overview of the engine and the accessory gearbox [3]. (b) Kinematics of the gearbox[3]. (c) Proposed method AD. (d) Spectral coherence [6]. (e) Integral of AD over a selected spectral amplitudes band. (f) Enhanced envelope spectrum [6]

The presence of the defective bearing is revealed by the vertical line at BPOO in both Fig.1 (c) and (d), in addition the proposed AD shows more clearly the sidebands, due to amplitude modulation, at plus/minus CO. Remarkably AD achieves this with only 50 threshold levels in the amplitude spectrum, versus 129 filters of ~200 Hz pass band used in the SC. Figures (e) and (f) confirm the better performance of AD where the signal to noise ratio of the sidebands is higher than in the SC.

In conclusion the Amplitude cyclic frequency Decomposition performed well in a real world scenario, detecting a defective bearing from vibration data collected from an accelerometer mounted on a civil aircraft engine during a run up test. The proposed algorithm is easy to automate, with only the number of threshold levels to be selected and it has low computational complexity, therefore is a good candidate to be deployed in a condition monitoring unit.

References:

[1] R.B. Randall, Vibration-based Condition Monitoring- Industrial, Aerospace and Automotive Applications, J. Wiley and Sons, (2012)
[2] V. Girondin, K. M. Pekpe, H. Morel, J.P. Cassar, Bearings fault detection in helicopters using frequency readjustment and cyclostationary analysis, Mechanical Systems and Signal Processing, 38(2). (2013)
[3] J. Antoni, J. Griffaton, H. André, L. D. Avendaño-Valencia, F. Bonnardot, O. Cardona-Morales, G. Castellanos-Dominguez, A.P. Daga, Q. Leclère, C. Molina Vicuña, D. Quezada Acuña, A.P. Ompusunggu, E. F. Sierra-Alonso, Feedback on the Surveillance 8 challenge: Vibration-based diagnosis of a Safran aircraft engine, Mechanical Systems and Signal Processing, in Press, (2017)
[4] https://www.gov.uk/aaib-reports/2-2011-aerospatiale-eurocopter-as332-l2-super-puma-g-redl-1-april-2009 (last visited April 2017)
[5] F. Elasha, M.Greaves, D. Mba A. Addali, Application of Acoustic Emission in Diagnostic of Bearing Faults within a Helicopter Gearbox, Procedia CIRP 38 (2015): 30-36.
[6] J. Antoni, G. Xin, N. Hamzaoui, Fast computation of the spectral correlation, Mechanical Systems and Signal Processing, 92, (2017)

Structural Design, Manufacturing and Instrumentation of rotor blades

Samuel C. R. Furtado[1], Antonio Filippone[2], Nicholas Bojdo[2], Constantinos Soutis[1]

samuel.furtado@manchester.ac.uk

[1]*Northwest Composite Centre, School of Materials, The University of Manchester*
[2]*School of Mechanical Aerospace & Civil Engineering, The University of Manchester*

Abstract

A consortium of comprising research centres and companies was established to develop and manufacture a state-of-art rotor rig for rotorcraft blades wind tunnel testing. A four-blade configuration was considered. One important task on the project was to design and manufacture instrumented helicopter and tilt rotor blades that will be used to demonstrate the rotor rig capabilities.

In the present work, the steps and challenges faced during the blades design, manufacturing and instrumentation are discussed.

Taking into consideration the wind tunnel conditions and the rotor jig expected capabilities, the aerodynamic profiles were generated. The Mach number scaled profiles obtained are expected to generate 2.5 KN (at 2500rpm) and 3kN (at 3000 rpm) of trust for the helicopter and the tilt rotor blades, respectively.

Regarding the mechanical design and manufacturing, the blades final solutions must provide components capable to generate the aerodynamic profile and simultaneously fulfilling other requirements (e.g. level of noise and comfort and/or other special applications capabilities). One important requirement was the maximum permissible radial hub load, which was set at 15 kN. This means that the design solution and material must be selected in order to maintain the mass and radius of gyration low enough to remain within the centrifugal load limit. Therefore, the challenge was to select material and configurations that simultaneously ensure low mass, effective mass distribution and not exceed material strength.

To facilitate control of design *lumped mass approximation*, based on a simple dynamic relationship between the rotor blade mass, radius of gyration and centrifugal load, was used to create a constraint chart.

The blades had also to be instrumented. The instrumentation will be used to capture the blades modes of shapes. In order to have the lowest perturbation possible in the aerodynamic behaviour, internal instrumentation was considered. This requires the blades to have a hollow cross-section.

Using the lumped mass approximation, an initial 'target' weight was established. Then, by using ABAQUS software finite element analysis (FEA) was performed to determine whether a failure is expected or not. Additionally, the design was also changed in order to reduce the blade deflections. After several iterations, the optimized solutions presented in the figure 2 were achieved.

For the tilt rotor blades, the solution consisted in a composite aerofoil skin, a D-spar, an aluminium metal root fitting and maraging steel shear pin and collar rings. The D-spar composed by a composite skin and a foam core, was used to increase the blade stiffness without compromising the weight.

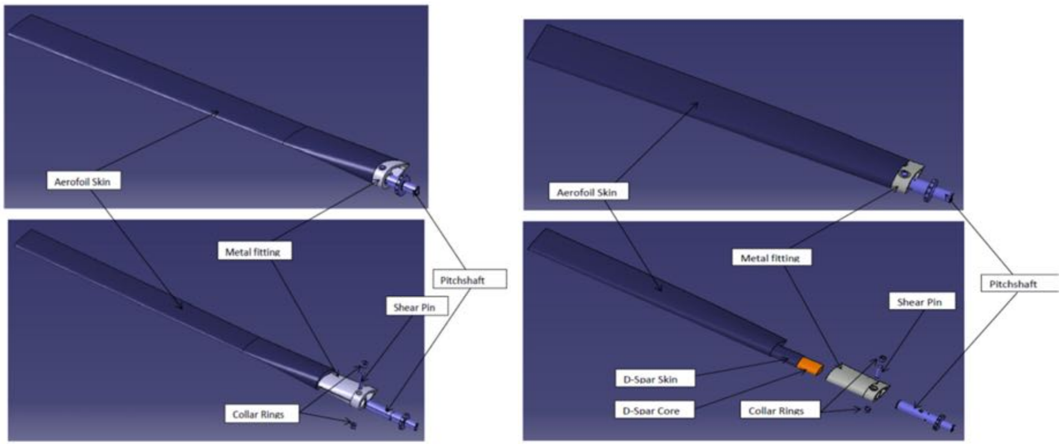

Figure 2 - Blades design solutions: Helicopter (left); Tilt rotor (rigth).

In turn, the helicopter blade solution was similar to the tilt rotor one, apart from the absence of a D-spar. The thinner aerofoil cross-section in this case, made the use of a D-spar impractical. To overcome this constraint, changes in the composite skin lay-up were considered, where different ply orientation and higher number of plies were selected.

The necessity for an internal instrumentation determines that blades have to be manufactured in two separate halves and bonded together after the instrumentation.

The use of composites materials, enabled a successful design and manufacturing of instrumented blades, where the weight requirement was fulfilled and allowing the wind tunnel constraints to be met. The composite materials also provided bigger design flexibility, enabling the designer to ‘tailor’ some material properties in accordance with the requirement. However, the manufacturing and instrumentation present several challenges, especially due to small sizes presented in this case. Special tools and equipment may be required for trimming and assembling.

Figure 3 – Rotor rig assembly.

Keywords: Rotorcraft blades design; Rotorcraft blades manufacturing; Rotorcraft blades instrumentation; Composite materials blades; Wind tunnel test.

An update on the BLADESENSE project

Dr. Mudassir Lone (Cranfield University)

The primary objectives of the proposed work are to address the challenges of deploying fibre-optic sensors within the harsh environment of a spinning rotor hub, obtaining accurate and robust data and integrating the sensory information with a helicopter health monitoring system. The very novel approach is the direct shape measurement of helicopter blades using optical fibre interferometry. Additional static and dynamic testing will underpin the feasibility of this novel approach. The overall aim is to use an on board system to compare mathematical models of a healthy rotor blade with the real-time sensory data from the fibre-optic instrumentation.

The proposed work is motivated by the need for accurate and timely servicing of flight critical components, such as the main and tail rotor blades. Progress in the area of helicopter maintenance, repair and servicing is severely limited by the lack of knowledge about the actual loading environment and resulting blade deformations. Current servicing practices are heavily reliant on conservative guidelines defined during the design and development phases of the rotorcraft. These are obtained from basic loading tests done on a whirl rig, from which the anticipated working life is extrapolated. This method has to employ significant conservatism to account for unknown variables. Detailed knowledge of the operational loads could be used to reduce the need for such conservatism, thus reducing servicing intervals and increasing blade life. Surface mounted strain gauges have been used to measure strain and infer deformation. These gauges are expensive to install, delicate and not suited for the hostile environment encountered on a rotor hub in operational use. The proposed research aims to address this fundamental limitation by developing a novel instrumentation system that will directly measure the deformation and thus allow health monitoring.

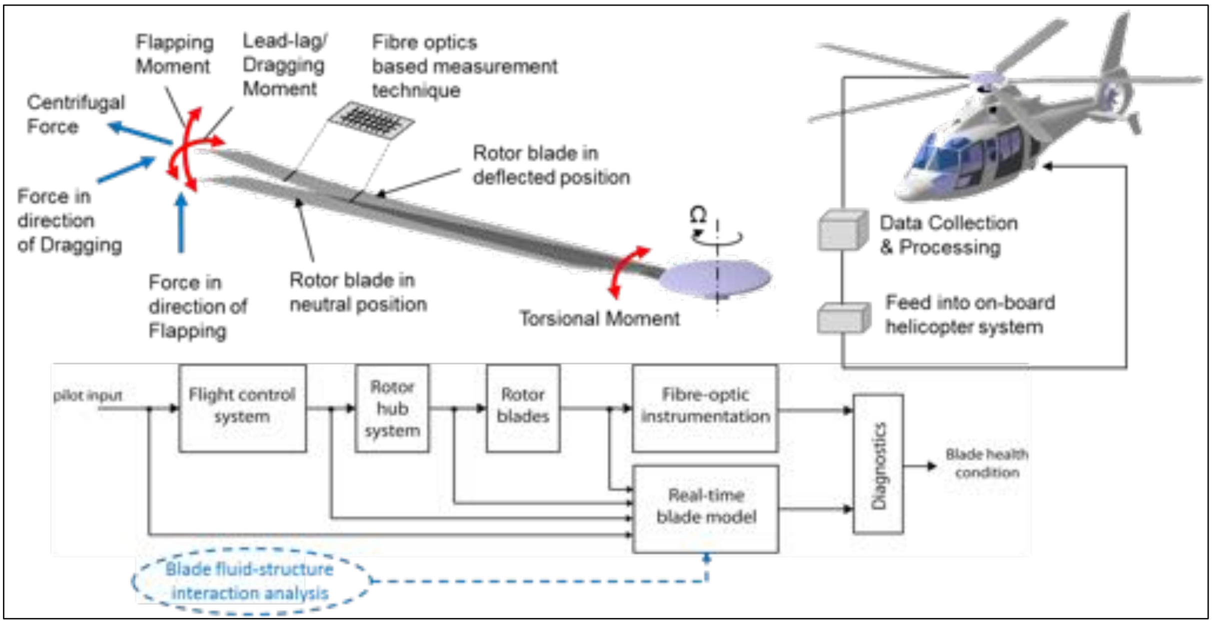

Figure 1: BLADESENSE development overview

The presentation will provide an overview of the developments in the project over the last two years, as shown in Figure 1. Especially, focusing on key areas of (a) structural modelling of flexible rotor blades, (b) 6 DoF modelling of helicopter flight mechanics, (c) fibre-optic sensing technology and, (d) flight test methods. The presentation will conclude by outlining future work planned over the last half of the project duration.